FINITE ELEMENT ANALYSIS OF ELASTOMERIC BEARINGS UNDER CYCLIC SHEAR LOADING

by

Berkay BİÇER

B.S, Mechanical Engineering, TOBB ETU University, 2020

Submitted to the Institute for Graduate Studies in
Science and Engineering in partial fulfilment of
the requirements for the degree of
Master of Science

Graduate Program in Mechanical Engineering

Boğaziçi University

2023

ACKNOWLEDGEMENTS

I would like to thank my supervisor Prof. Şebnem Özüpek for her guidance and support throughout my thesis study. I would also like to thank defense jury members Prof. Erdem Acar and Assist. Prof. Esat Selim Kocaman for the review of my thesis and TÜBİTAK BİDEB 2210-A University Scholars Research Project scholarship throughout my postgraduate studies.

Finally, I would like to thank my parents Kadriye and Atilla Biçer, and my sister Simay Biçer for their love.

ABSTRACT

FINITE ELEMENT ANALYSIS OF ELASTOMERIC BEARINGS UNDER CYCLIC SHEAR LOADING

The study is concerned with the analysis of high damping rubber isolation bearings under seismic excitations. High damping rubber (HDR) plays an important role in seismic isolation systems due to its good damping capability and long service life. Accurate representation of its mechanical behavior is essential for the simulation of the high damping rubber bearings (HDRB).

The emphasis of the study is on the formulation of a constitutive model for HDR that accounts for large strains, cyclic loading, hysteresis and rate dependence while being computationally efficient. The calibration of the constitutive model and its validity are done using experimental data available in the literature. The constitutive model for HDR is used in the analysis of HDRB. 2D and 3D finite element models of bearing are developed and the response for compression and shear loadings are predicted. The sensitivity of the response to various parameters is investigated.

The agreement of the predictions with the limited test data on HDRB is encouraging. Bearing stiffness and damping ratio are calculated within ranges available in the literature. The effect of loading rate on the hysteresis amount follows the trend observed in experiments. The methodology developed in the thesis can be applied to different isolators. The computational model can be used to understand the isolator’s behavior in detail without numerous tests and procedures.

ÖZET

ELASTOMER İZOLATÖRLERİN ÇEVRİMSEL KESME YÜKLEMELERİ ALTINDA SONLU ELEMAN ANALİZLERİ

Sismik uyarımlar altında elastomer mesnetlerin analizi üzerine çalışılmıştır. Yüksek sönümleyici kauçuk (HDR), iyi sönümleme kabiliyeti ve uzun hizmet ömrü nedeniyle sismik izolasyon sistemlerinde önemli bir rol oynar. Elastomer mekanik davranışının doğru temsili, mesnet simülasyonu için esastır.

Çalışmanın odağında, HDR malzeme modelinin büyük gerinimleri, çevrimsel yüklemedeki histerezisi ve yükleme hızına bağımlılığı göz önüne alması, aynı zamanda da hesaplamaya uygun olması yer almaktadır. Modelin kalibrasyonu ve doğrulanması, literatürde bulunan deneysel veriler kullanılarak tamamlanmıştır. Elde edilen malzeme modeli kullanılarak izolatörlerin basma ve kesme yükleri altındaki mekanik davranışı iki ve üç boyutlu sonlu elemanlar analizi ile öngörülmüştür. Ayrıca analiz çıktılarının çeşitli parametrelere duyarlılığı incelenmiştir.

Tahminlerin elastomer mesnet ile ilgili sınırlı test verisiyle uyumlu olması cesaret vericidir. Öngörülen mesnet sertliği ve sönüm oranı literatürde mevcut olan aralıklardadır. Yükleme hızının histerezis miktarı üzerindeki etkisi, deneylerde gözlemlenen eğilimi izlemektedir. Tezde geliştirilen metodoloji farklı izolatörlere uygulanabilir. Hesaplamalı model, izolatörün davranışını çok sayıda test ve prosedür olmaksızın ayrıntılı olarak anlamak için kullanılabilir.

TABLE OF CONTENTS

LIST OF FIGURES

LIST OF TABLES

LIST OF SYMBOLS

C	Cauchy-Green deformation tensor
E	Elastic modulus
E'	Hardening modulus
E_I	Lagrangian finite strain tensor
K_0	Initial bulk modulus
S	Second Piola-Kirchhoff stress
SF	Shape factor

ε	Nominal strain
γ	Shear strain
μ	Coefficient of friction
μ_0	Initial shear modulus
λ	Stretch
ν	Poisson’s ratio
σ	Normal stress

LIST OF ACRONYMS / ABBREVIATIONS

2D	Two dimensional
3D	Three dimensional
FE	Finite element
HDR	High damping rubber
HDRB	High damping rubber bearing
LRB	Lead reinforced rubber bearing
NR	Natural rubber
NRB	Natural rubber bearing
SF	Shape factor

1. INTRODUCTION

Elastomeric bearings are layered support structures used for providing axial, shear and rotational support. Usage of bearings increases service life, reliability, safety and reduces maintenance costs. Accustomed versions of these bearings are natural rubber bearings (NRB), lead rubber bearings (LRB) and high damping rubber bearings (HDRB). Laminated rubber bearings are widely used in seismic isolation industry. HDR and NR are selected due to their damping potential and horizontal flexibility. Although NR can be further improved by adding extra fine carbon particles and oils, HDR performs better for damping [1].

HDRB are composed of high damping rubber material and metal supports called liners. Liners are primarily used for lateral stiffness while HDR is responsible for energy dissipation. Figure 1.1 is an example drawing of a rubber isolator.

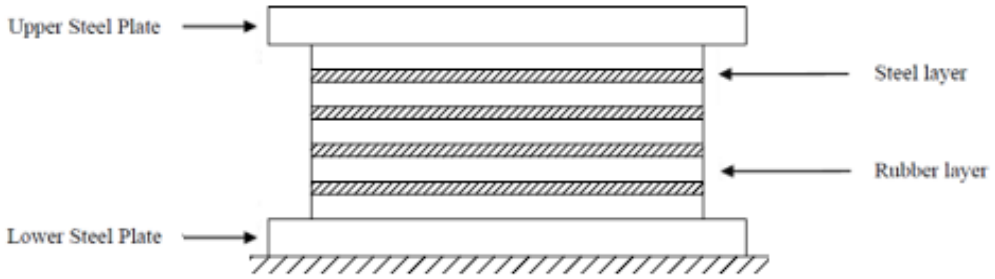

Figure 1.1. Elastomeric isolator.

When a structure is subject to seismic movements, HDR generally shows large deformations, hysteresis, time dependence, and softening. Each of these effects have implication on stress response of the rubber.

Elastomer materials generally undergo large deformations. Large deformation theory is used when strains or rotations are high enough to overrule infinitesimal strain theory. This geometric nonlinearity needs to be taken into account for accurate representation of the elastomer behavior.

Hysteresis is a material nonlinearity observed in cyclic response of elastomer. It is a measure of the energy dissipated by the internal friction of the material during loading and unloading.

Rate dependence in rubber behavior is critical for obtaining accurate stress-strain curves. This aspect is generally implemented using viscoelastic material model [2]. Characterization of elastomers as a viscoelastic material requires extensive testing which typically is not available for isolation bearing.

Softening of rubber is observed as the stress drop between successive loading cycles. This effect is called Mullin's effect. To form a better understanding of Mullin's effect, several physical tests are present in the literature on chain breakage at the interface of the rubber and filler materials, molecule slippage, chain disentanglements and composite structure formations. This material nonlinearity is important during the initial cycles of loading and becomes negligible after few cycles.

1.1. Literature Review

Literature is explored for gaining detailed information about HDR, HDRB and isolation systems. After these main headings, more detailed investigation is followed as critical effects in rubber behavior, hyperelastic and viscoelastic material model, rubber hysteresis, stiffness and energy dissipation.

In the study by Amin et. al. [3], viscoelastic effects for NR and HDR are investigated using Zener model. Experimental results on relaxation tests and monotonic uniaxial tests at different strain rates are compared with the simulation. It is stated that HDR shows important nonlinear effects in monotonic loads and hysteresis effects in cyclic loads. Test data for compression and shear behavior of the HDR are used for verification and validation of the findings in this thesis.

In the study by A. Amin [4], viscohyperelasticity model is formed and nonlinear dependence of viscosity through internal variables is investigated. 2D and 3D FEM model results are compared with full scale HDRB test outputs for different shape factors and shear strain rates. Both compression and combined compression and shear are investigated.

In the study by A. Emran [2], 2D FEM model of a rubber bearing isolator is formed. Behavior of the material is modelled by combination of viscoelastic (Prony series) and the hyperelastic (Ogden model) approaches. Hysteresis behavior is tested for multiple cycles and various shear displacements.

In the study by A. R. Bhuiyan [5], cyclic shear, multi-step relaxation and simple relaxation tests are done on HDRB. Rate dependence is measured, ranging from equilibrium to instantaneous loads. Elasto-viscoplastic material model is used. For this, Maxwell viscoelastic model is modified to include nonlinear rate dependent effects.

In the study by K. N. Kalfas [6], Ogden hyperelastic material model is used for the rubber. This work investigates a method to implement hysteresis effects in hyperelastic material and predict damping response. Stiffness, dissipation capacity and stress levels of the bearing are measured under various compression levels and boundary conditions.

Study of N. Murota [7] is an experimental work that investigates HDRB data in terms of geometry, compressive stresses, damping ratio, stiffness and strain limits. Extensive design and material parameters are listed. Cyclic experimental tests are performed for understanding effects of rubber aging, operating temperature and manufacturing tolerances on bearing performance.

Study of M. Saedniya [8] investigates cyclic behavior of HDRBs and LRBs through finite element modeling and testing. Tests include uniaxial tension/compression, equibiaxial tension/compression, planar shear and volumetric tension/compression. Yeoh strain energy function is calibrated and is shown to predict the effective stiffness measured in the experimental data the best as compared to other hyperelastic material models such as

Mooney-Rivlin and Ogden forms. It is mentioned that the softening effect during loading and unloading could not be simulated by the hyperelastic model.

In the study by D.A. Nguyen [9], cyclic experimental tests on HDRBs at changing temperatures and shape factors are done. A rheology model is formed for investigating rate dependence and compared with experimental outputs. Numerical model parameters are calculated from equilibrium multi-step relaxation tests. Stress level of the bearing is seperated into nonlinear elasto-plastic, elastic and visco-elasto-plastic components. Importance of Mullins, self-heating and temperature history effects are mentioned for future work.

As most of the references point out, hysteresis behavior of rubber still needs extensive research and requires high accuracy model outputs under combined shear and compression loading. Hyperelastic material model performance and rate dependence for cyclic loads need to be evaluated for rubber. This work focuses on these aspects to contribute to research on how accurately HDRB behavior can be modelled. Large deformation analysis is done with the usage of hysteresis and hyperelastic model for cyclic loading.

Cyclic compression and shear loading response of high-damping rubber bearings with steel plates are investigated via finite element method in this thesis. Data for material properties, geometry and loading are selected from literature based on industrial usage and previous experimental works.

1.2. Objectives of the Thesis

Main objective of the thesis is to simulate the cyclic behavior of high damping rubber bearings. The rate-dependent attributes of HDR and HDRB are investigated for compression and shear loadings via finite element method. The use of accurate material properties, large deformation and hysteresis is emphasized in order to reach realistic results. A constitutive

model combining hyperelasticity and rate dependence is used. The model parameters are determined for test data available in the literature.

The effects of the following properties on the bearing response are investigated,

- Rubber compressibility,
- compressive loading magnitude,
- Loading rate,
- Shape factor.

Effects of two and three dimensional modeling on results are also explored. Static analysis with implicit time integration is used and stress analysis software is selected as ABAQUS [10].

In Chapter 1, a brief introduction to the isolation bearing types is mentioned. Literature research, objectives and outline of the work is given.

Chapter 2 forms the theoretical background on rubber and bearing analysis. This includes hyperelasticity, shape factor, compressibility and energy dissipation calculation.

Chapter 3 mainly focuses on the modeling of the mechanical behavior of rubber, calibration of the selected material model and validation of the results against test data. The resulting model is used in the deformation analysis discussed in the remainder of the thesis.

Chapter 4 presents analysis of a small size bearing with shape factor 5. The effects of strain rate and compressibility level on bearing stresses are investigated.

Chapter 5 describes a full-size industrial bearing. The bearing is analyzed under various loading conditions and the results are compared with experimental data. Effects of compressibility and strain rate are investigated.

Chapter 6 presents conclusion part that summarizes modeling, comparison and observations. Effectiveness of the model, accuracy ranges, and outputs are briefly reviewed.

2. THEORY

The use of finite strain theory is essential in description of rubber mechanical behavior and stress analysis of elastomeric isolators. Elastomers require this type of modeling to generate accurate results. Brief summary of the concept is in this section.

2.1. Finite Strain Theory

In finite strain theory, forming relations for undeformed and deformed bodies is critical. Displacement field is expressed in terms of undeformed configuration coordinates $\mathbf{X}$, and deformed configuration coordinates $\mathbf{x}$ in

$$\mathbf{u}(\mathbf{X}) = \mathbf{x}(\mathbf{X}) - \mathbf{X}. \tag{2.1}$$

Continuum motion is mathematically modelled by deformation gradient tensor $\mathbf{F}(\mathbf{X})$ which relates undeformed configuration to deformed configuration where

$$d\mathbf{x} = \mathbf{F}(\mathbf{X})\, d\mathbf{X}. \tag{2.2}$$

The symmetric part of deformation may be expressed in terms of Cauchy-Green deformation tensor or Green's deformation tensor $\mathbf{C}$ can be written as

$$\mathbf{C} = \mathbf{F}^T\mathbf{F} = \mathbf{U}^2. \tag{2.3}$$

Invariants of $\mathbf{C}$ are further used for strain energy density function.

Strain tensor represents variance of the movement from rigid body displacement locally. Lagrangian finite strain tensor is defined in terms of $\mathbf{C}$ as

$$\mathbf{E_I} = \frac{1}{2}\,(\mathbf{C} - \mathbf{I}). \tag{2.4}$$

2.2. Hyperelasticity

Hyperelasticity uses strain energy function for derivation of stress-strain relation. Strain energy W defines stored energy per unit volume as a function of strain [10]. Second Piola-Kirchhoff stress **S**, is derived from the energy density W, as

$$\mathbf{S} = 2\frac{\partial W}{\partial \mathbf{C}}. \tag{2.5}$$

Large deformations of high damping rubber can be modelled by using Yeoh strain energy function due to its performance computationally and predictive capability for multiaxial loadings [11]. Yeoh model is a phenomenological model.

Original Yeoh function is expressed for an incompressible material as

$$U = C_{10}(I_1 - 3) + C_{20}(I_1 - 3)^2 + C_{30}(I_1 - 3)^3. \tag{2.6}$$

General form of the strain energy function for compressible rubbers is

$$\begin{aligned} U = {} & C_{10}(I_1 - 3) + C_{20}(I_1 - 3)^2 + C_{30}(I_1 - 3)^3 + \frac{1}{D_1}(J^{el} - 1)^2 \\ & + \frac{1}{D_1}(J^{el} - 1)^4 + \frac{1}{D_1}(J^{el} - 1)^6 \end{aligned} \tag{2.7}$$

and J^{el} can be calculated as

$$J^{el} = I_3. \tag{2.8}$$

C_{i0} and D_i are temperature dependent material parameters, I_1 is the first and I_3 is the third invariant of Cauchy Green deformation tensor [12]. I_1 can be written as

$$I_1 = \lambda_1^2 + \lambda_2^2 + \lambda_3^2 \tag{2.9}$$

where λ_i are principle stretches.

2.3. Shape Factor

The shape factor (SF) is defined as the ratio of the loaded area to the load free area. The shape factor of a bearing is a measurement of how thin the rubber layer is. SF for rectangular geometry is calculated as

$$Shape\ Factor = \frac{ab}{2(a+b)t}. \tag{2.10}$$

a and b are side lengths of the rubber and t represents thickness.

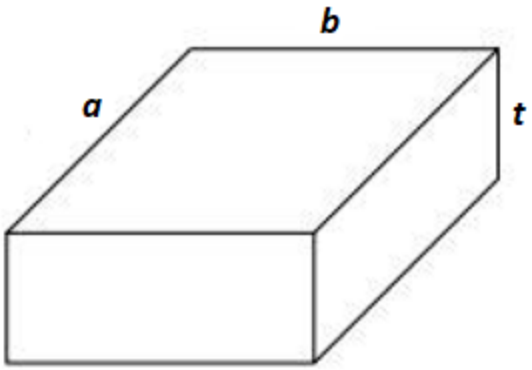

Figure 2.1. Rectangular bearing geometry.

For isolation bearings, shape factor values between 5 to 20 are widely used [12]. Although damping is directly related to material property, shape factor has an effect on the behavior. According to [11], KL401 rubber with shape factor larger than 20 is observed to have good isolation in horizontal loads.

2.4. Compressibility

Compressibility is defined as instantaneous relative volume change of a material under pressure change. Typically, rubber has a nearly incompressible behavior. Since it is rather

difficult to measure its volumetric response, rubber is computationally modeled as incompressible. On the other hand, when explicit solution techniques are used it is not possible to model the rubber as incompressible. It is therefore important to determine the effect of compressibility on the predicted response of the rubber as well as the bearing. In this work, various levels of compressibility are considered and the effects on stiffness and damping ratio are noted.

In the study, compressibility is defined as the ratio of the initial bulk modulus K_0 to the initial shear modulus μ_0 and expressed as

$$Compressibility = \frac{K_0}{\mu_0}. \tag{2.11}$$

Relation between initial bulk modulus, initial shear modulus and Poisson's ratio are written as

$$\nu = \frac{3K_0/\mu_0 - 2}{6K_0/\mu_0 + 2}. \tag{2.12}$$

Table 2.1. Compressibility and Poisson's ratio relations.

κ_0/μ_O	ν_0
10	0,452
20	0,475
50	0,49
100	0,495
2000	0,49975
Infinite	0,5

2.5. Hysteresis

Hysteresis in this work, refers to the stress difference between the loading and unloading stages in a cyclic loading. Difference between the two curves is the dissipated energy due to internal friction during one cycle. A typical hysteresis loop is shown in Figure 2.2.

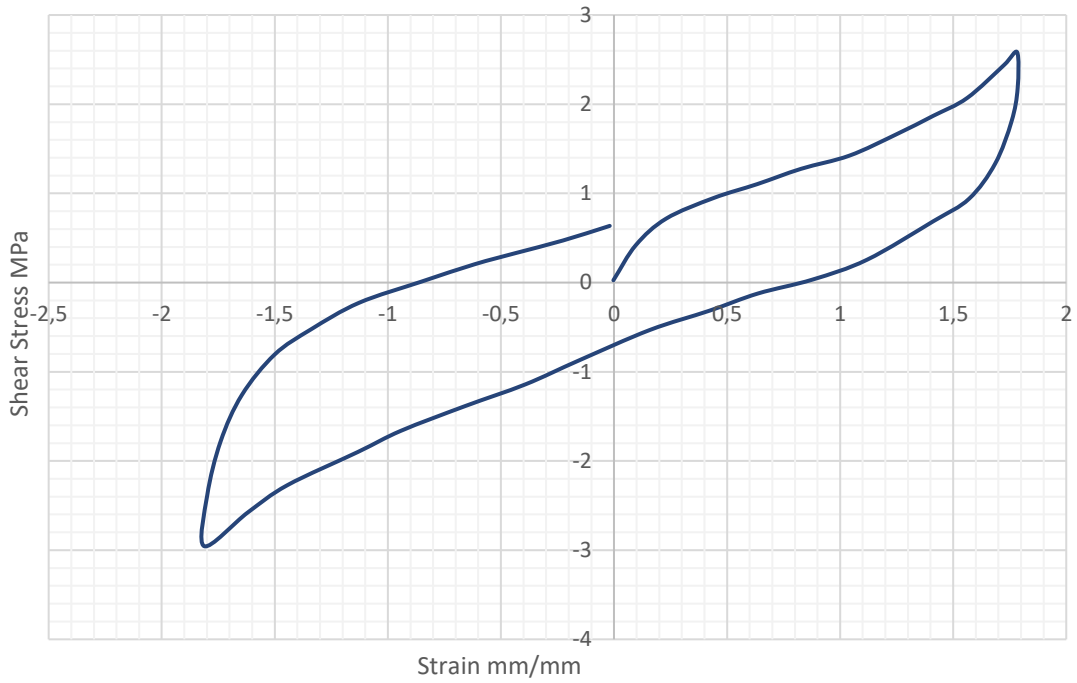

Figure 2.2. HDRB under cyclic shear loading with strain rate of 0.05/s [5].

Since hysteresis curve is directly related to damping ratio, high damping rubber is widely used for isolation of vibrations and sound.

From modeling perspective, viscoelastic material model is successful in creating hysteresis behavior for rubber material. On the other hand, viscoelastic model requires various tests for calibration which were not available for HDR studied in the thesis. Therefore, a nonlinear, strain rate dependent model is used for reproducing hysteretic behavior of elastomers under cyclic loading [13].

Nonlinear strain-rate dependence is modelled by dividing the mechanical response into that of two networks. The equilibrium response of network A and time dependent response of network B. Network A response represents the state at the end of long-time stress relaxation of the material. B is the time dependent network and captures the nonlinear rate dependent deviation from the equilibrium state. Summation of two responses gives the total stress. Deformation gradient **F** acts on both of the networks and for network B is divided into elastic and inelastic parts.

Network A stress tensor in principle directions is calculated by

$$\sigma_{i_A} = C_R^{(A)}\sqrt{N_A}\frac{\left(\lambda_{i_A}\right)^2 - \left(\lambda_{chain_A}\right)^2}{\lambda_{chain_A}}\mathcal{L}^{-1}\left(\frac{\lambda_{chain_A}}{\sqrt{N_A}}\right) + B\,ln\left(\sqrt{I_{3_A}}\right). \quad (2.13)$$

Stress on the network B be can be calculated in the same manner as network A and expressed as

$$\sigma_{i_B} = C_R^{(B)}\sqrt{N_B}\frac{\left(\lambda_{i_B}\right)^2 - \left(\lambda_{chain_B}\right)^2}{\lambda_{chain_B}}\mathcal{L}^{-1}\left(\frac{\lambda_{chain_B}}{\sqrt{N_B}}\right) + B\,ln\left(\sqrt{I_{3_B}}\right), \quad (2.14)$$

$$\lambda_{chain_A} = \frac{1}{\sqrt{3}}\left[\left(\lambda_{1_A}\right)^2 + \left(\lambda_{1_A}\right)^2 + \left(\lambda_{1_A}\right)^2\right]^{1/2}, \quad (2.15)$$

$$\mathcal{L}(x) = cot\,h(x) - \frac{1}{x}. \quad (2.16)$$

σ_i represents stress levels of networks. Both stresses are calculated by the formula called eight chain network [13]. Stretch at each individual chain is given as a function of principle stretches λ_i. I_i are the principle stretch invariants. $\mathcal{L}^{-1}\left(\lambda_{chain}/\sqrt{N}\right)$ are the reverse Langevin functions. N_A and N_B are the limiting of chain stretches, B is the bulk modulus. C_{R_A} and C_{R_B} are the initial modulus. C_{R_A} is defined as

$$C_R^{(A)} = \frac{nkT}{3} \quad (2.17)$$

where k is the Boltzmann constant, n is the number of chains per unit volume and T is the temperature.

Network B effective creep strain rate is calculated as [14]

$$\dot{\varepsilon}^{cr} = A[\lambda_B^{cr} - 1 + E]^C(\sigma_B)^m, \quad (2.18)$$

$$\sigma_B = \sqrt{\frac{3}{2}\mathbf{S}_B : \mathbf{S}_B}\,. \tag{2.19}$$

$\lambda_B^{cr} - 1$ represents nominal creep strain, σ_B is effective stress and $\mathbf{S}_B$ is deviatoric Cauchy stress tensor for network B. Stretch for the network is expressed as

$$\lambda_B^{cr} = \sqrt{\frac{1}{3}\, I : \mathbf{C}_B^{cr}}\,, \tag{2.20}$$

$$\mathbf{C}_B^{cr} = \mathbf{F}_B^{cr^T}\, \mathbf{F}_B^{cr} \tag{2.21}$$

where $\mathbf{F}_B^{cr}$ is the inelastic part of deformation gradient in network B.

The model is micromechanically motivated, it is valid for large strains and it is computationally efficient. An example of model prediction is shown in Figure 2.3. [13] includes tests at different rates, relaxation, various carbon black levels.

The material model parameters to be determined from experiments are stress scaling factor, $S = C_R^{(A)}/C_R^{(B)}$, and effective creep strain parameters *A*, *E*, *C* and *m*. The calibration procedure is discussed in Section 3.1.2.

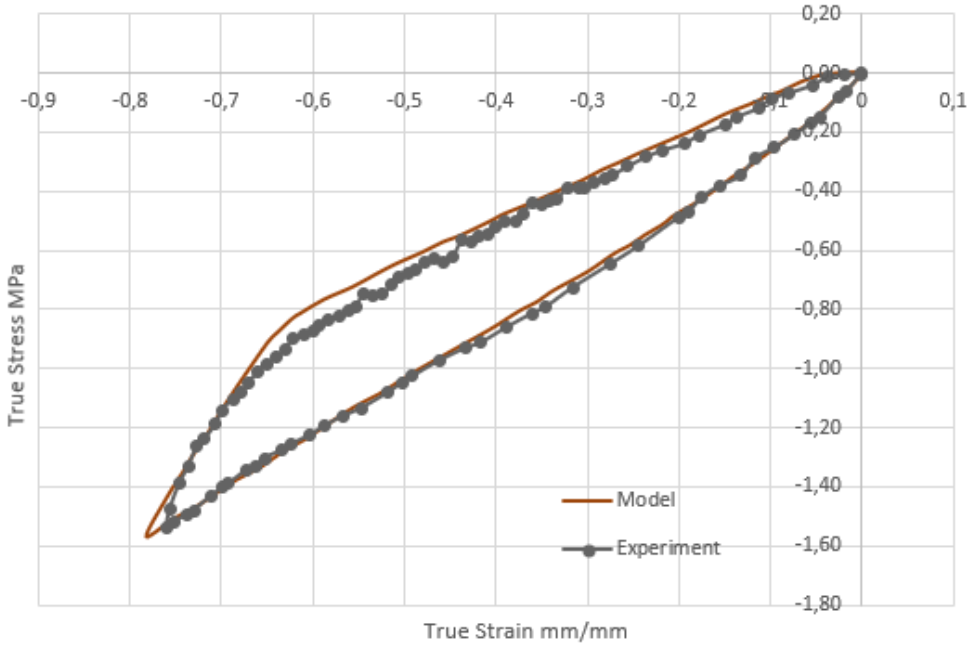

Figure 2.3. Stress strain curve of chloroprene rubber (15 pph) with strain rate of -0.01/s [13].

3. CONSTITUTIVE MODELING OF THE ELASTOMER

In this chapter, material model of HDR is presented. Particular emphasis is given to the cyclic loading simulation. Stress-strain and stiffness predictions are compared with experimental data. After validation of the material model for rubber, bearing models are examined in Chapters 4 and 5.

3.1. Material Model

HDR is represented with a strain rate-dependent model valid for large deformation. The model consists of elastic part defined through hyperelastic function and inelastic part that simulates hysteresis. For the hyperelastic function Yeoh energy formulation is used. In the following, the calibration of the Yeoh form and hysteresis model are described in detail.

3.1.1. Yeoh Parameters Calculation

Uniaxial compression test data at 0.001/s rate is used to calculate the Yeoh parameters [1]. The calibration as well as the evaluation of the model is done in ABAQUS [10].

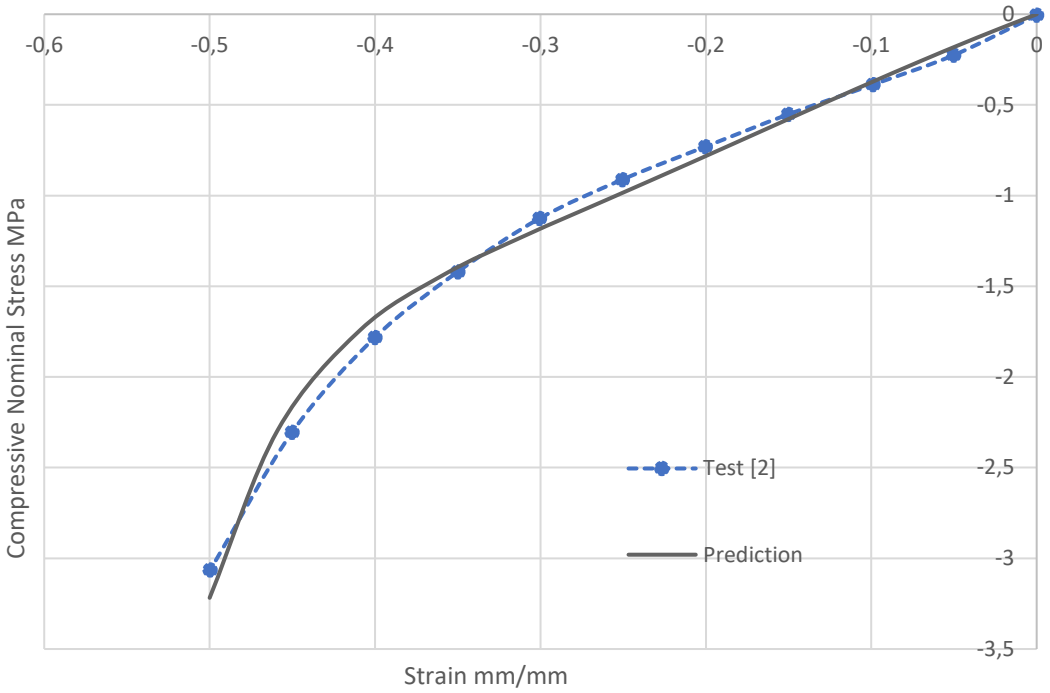

Figure 3.1. Test and model prediction for uniaxial compression at strain rate 0,001/s.

Table 3.1 shows the parameters, while Figure 3.1 shows the curve fit for uniaxial compression.

Table 3.1. Yeoh parameters for equilibrium ($\dot{\varepsilon} = 0.001/\mathrm{s}$).

	C10 (MPa)	C20 (MPa)	C30 (MPa)	D1, D2, D3
Equilibrium	0.577	-2.53E-01	0.11	0

3.1.2. Hysteresis Model Parameters

Elastomeric materials have rate dependent behavior and energy dissipation during loading and unloading. In this study, hysteresis material model developed by Bergström-Boyce [13] was used to account for rate dependent hysteretic behavior of HDR.

Table 3.2. Final hysteresis parameters at the end of calculations.

Stress Scaling Factor, *S*	Creep Parameter, *A*	Effective Strain Exponent, *m*	Creep Strain Exponent, *C*
9.42	0.1	4	-1

Parameters to be determined are the stress scaling factor, creep parameter, effective strain exponent and creep strain exponent, described in Section 2.5. Stress scaling factor is calculated as described in Section 3.1.2.1 and other time dependent parameters are determined by trial-error process using the finite element model shown in Figure 3.2. Calculation results are in Table 3.2.

To determine hysteresis parameters, a preliminary study on the effects of these parameters on the stress response was carried. Typical values for high damping rubber in the literature were used as shown in Table 3.3. First model uses recommended values in ABAQUS documentation [14]. Various creep parameters and effective strain exponents are selected from [13].

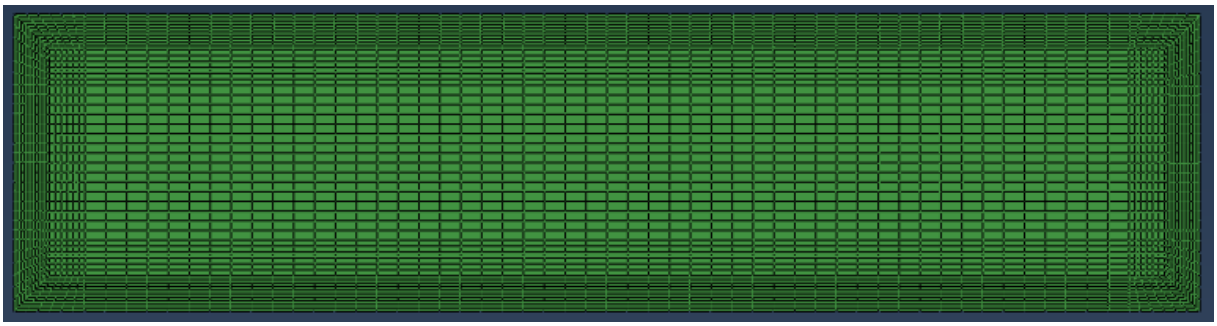

Figure 3.2. Rubber block geometry for hysteresis parameter study.

Table 3.3. Hysteresis parameter sets.

	Stress Scaling Factor, *S*	Creep Parameter, *A*	Eff Strain Exponent, *m*	Creep Strain Exponent, *C*
1	1.6	0.56	4	-1
2	3.2	0.56	4	-1
3	1.6	0.01	4	-1
4	1.6	7	4	-1
5	1.6	0.4	4	-1
6	1.6	0.56	5	-1
7	1.6	0.56	4	-0.5
8	2.6	0.01	4	-0.4
9	0.8	0.01	4	-0.4
10	3.2	0.01	4	-0.4

3.1.2.1. Stress Scaling Factor (S). Stress scaling factor identifies the ratio of stress transferred by network B to network A under instantaneous loading. Stress scaling factor has a major effect on the damping amount of the system. Damped energy is greater for a higher factor.

Stress scaling factor is calculated analytically. Formulas and theory given in the appendix chapter of [13] are used for calculation. Parameters used during calculation are expressed as

$$N^{(A)} = \frac{1}{3}\left[\lambda_{lim}^2 + \frac{2}{\lambda_{lim}}\right], \tag{3.1}$$

$$C_R^{(A)} = \frac{\sigma_{eq}}{\lambda^2 - \frac{1}{\lambda}} \sqrt{\frac{\lambda^2 + 2/\lambda}{3N^{(A)}}} \left[\vec{\mathcal{L}}\left(\sqrt{\frac{\lambda^2 + 2/\lambda}{3N^{(A)}}}\right)\right]^{-1}, \tag{3.2}$$

$$C_R^{(B)} = \frac{E_t}{3}\left[2\lambda^2 + \frac{1}{\lambda}\right]^{-1} - C_R^{(A)}, \tag{3.3}$$

$$S = \frac{C_R^{(B)}}{C_R^{(A)}}. \tag{3.4}$$

Requirements for calculation of stress scaling factor are λ_{lim}, λ, σ and E_t. λ, σ are strain and stress values taken from the monotonic equilibrium loading curve shown in Figure 3.3. E_t is the tangent modulus calculated from the slope of instantaneous unloading curve. λ_{lim} is the estimated maximum stretch.

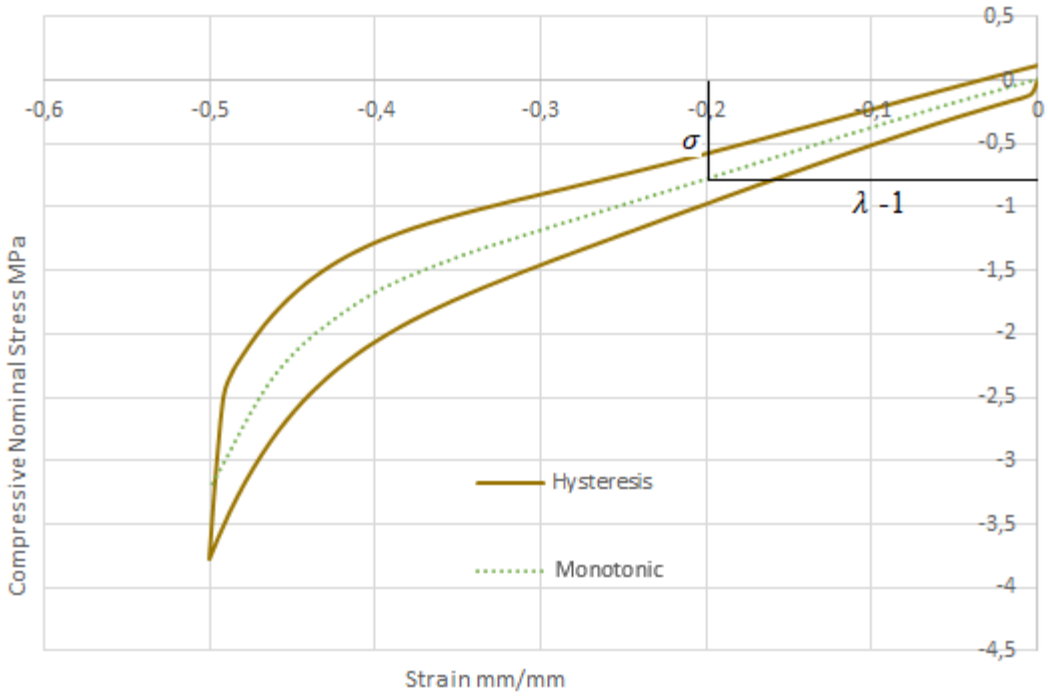

Figure 3.3. Compressive nominal stress-strain test data for equilibrium loading ($\dot{\varepsilon} = 0.001/\text{s}$).

Results are noted in Table 3.4.

Table 3.4. Stress scaling factor and calculation parameters.

σ (Pa)	λ	λ_{lim}	E_t (MPa)	$N^{(A)}$	$C_R^{(A)}$	$C_R^{(B)}$	Stress Scaling Factor
-7.30E+05	0.8	0.3	2.00E+07	2.25	2.53E+05	2.38E+06	9.42

Stress scaling factor is generally in the range of 0.77 [6] to 16 [8]. In [10], value 1.6 is recommended for common elastomers.

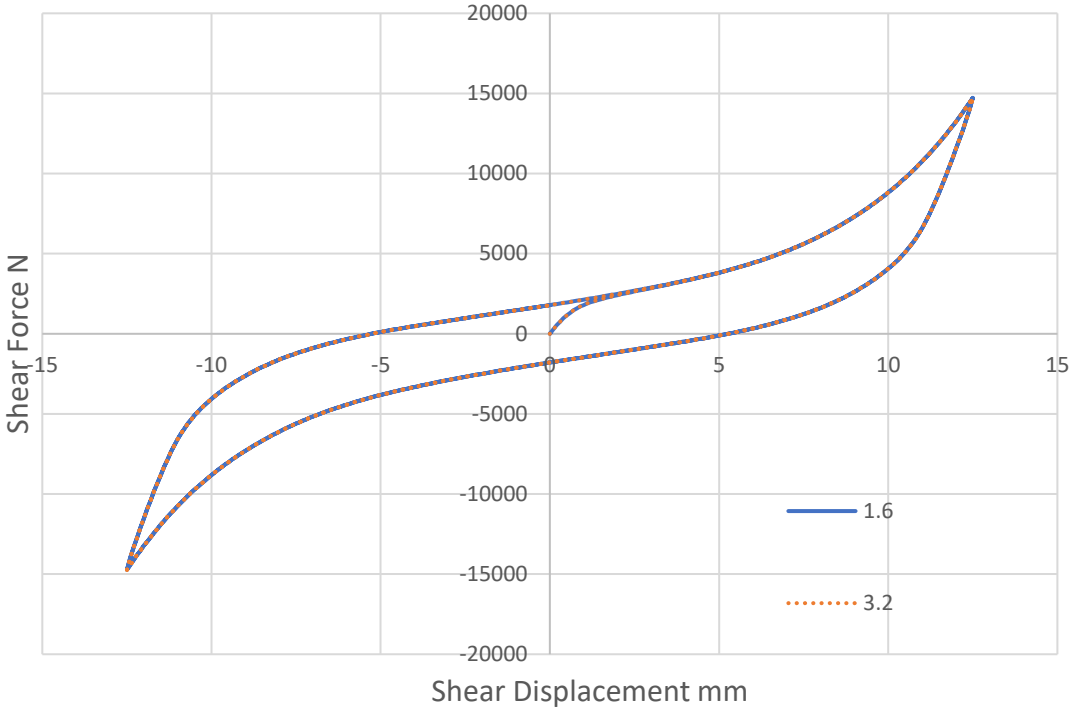

Figure 3.4. Stress scaling factor sensitivity for models 1, 2.

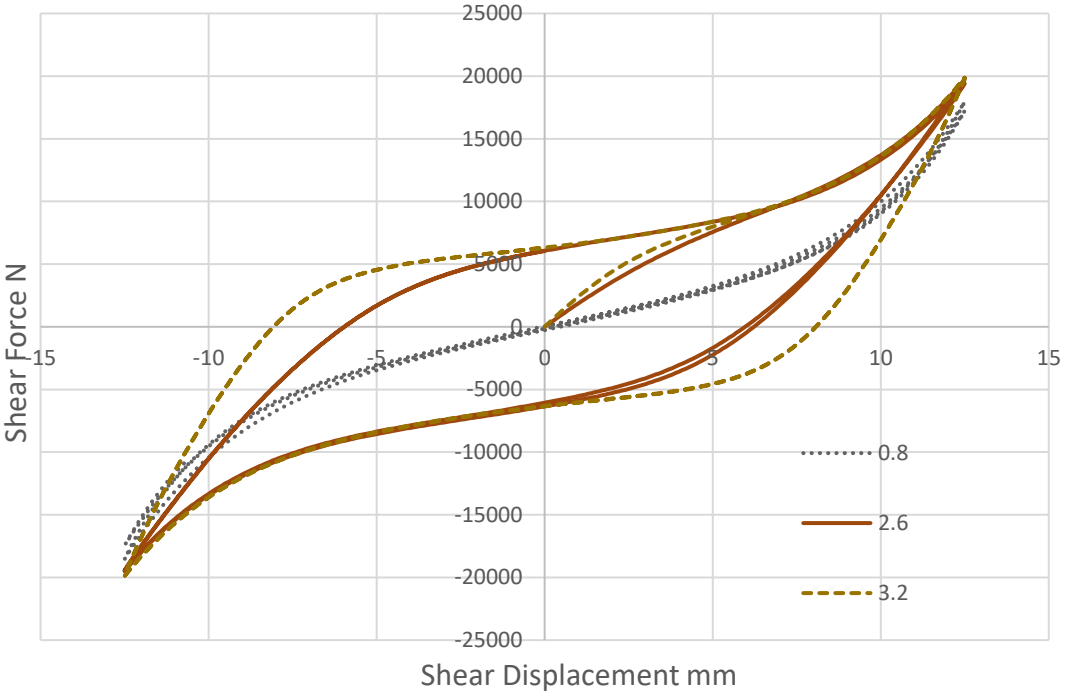

Figure 3.5. Stress scaling factor sensitivity for models 8, 9, 10.

For the selected set of creep parameters in Table 3.3, the response is not sensitive to stress scaling factor as seen in Figures 3.4 and 3.5. Therefore, lower creep parameter values were selected to evaluate the sensitivity to stress scaling factor. It was concluded that stress scaling factor does not have a notable effect on maximum-minimum stress values or stiffness.

3.1.2.2. Creep Parameter (A). Creep parameter is a constant used to calculate the effective creep strain rate.

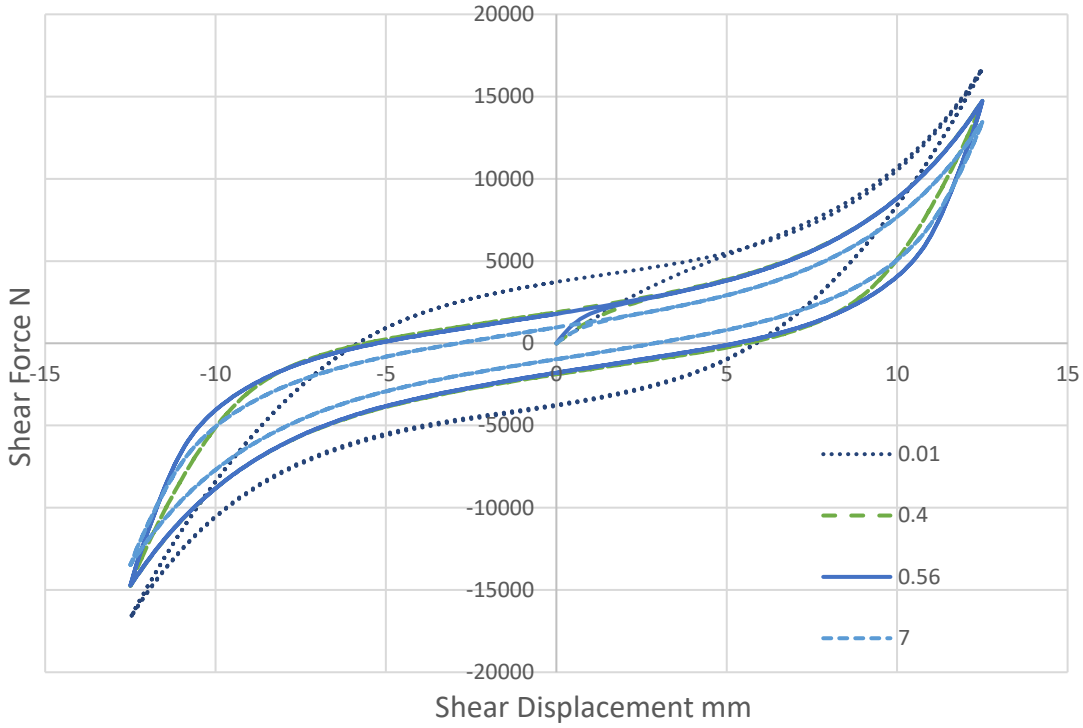

Figure 3.6. Creep parameter sensitivity for models 1, 3, 4, 5.

Figure 3.6 shows the effect of creep parameter on shear response. Model 4 with the largest creep parameter shows lower stresses at the maximum shear displacements. Increase in creep parameter lowers damping ratio and reduces stress value. Stiffness is also reduced with the increasing creep parameter.

3.1.2.3. Effective Strain Exponent (m). Effective strain is a positive exponent that characterizes effective stress dependence of the effective creep strain rate in network B. Effective strain exponent must be greater than 1. Reference models include values of minimum of 1.79 and maximum of 5.21. Typical value selection for common elastomer is 4 [10].

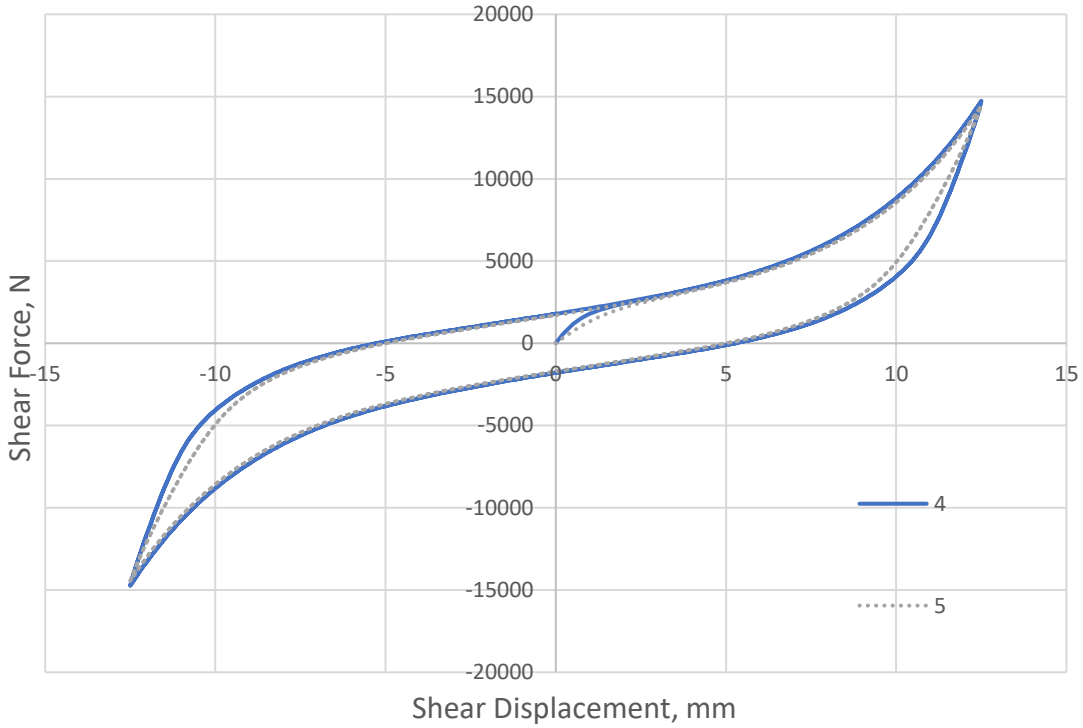

Figure 3.7. Effective strain factor sensitivity for models 1, 6.

Effective strain exponent sensitivity is investigated in Figure 3.7. Reducing this parameter results in lower damping amounts. Change in the damping ratio is less than 10%. Stress and stiffness levels are the same.

3.1.2.4. Creep Strain Exponent (C). Creep strain exponent characterizes the creep strain dependence of the effective creep strain rate in network B. Creep strain exponent must be in the range of -1 to 0, and it is recommended to be selected closer to -1 [10].

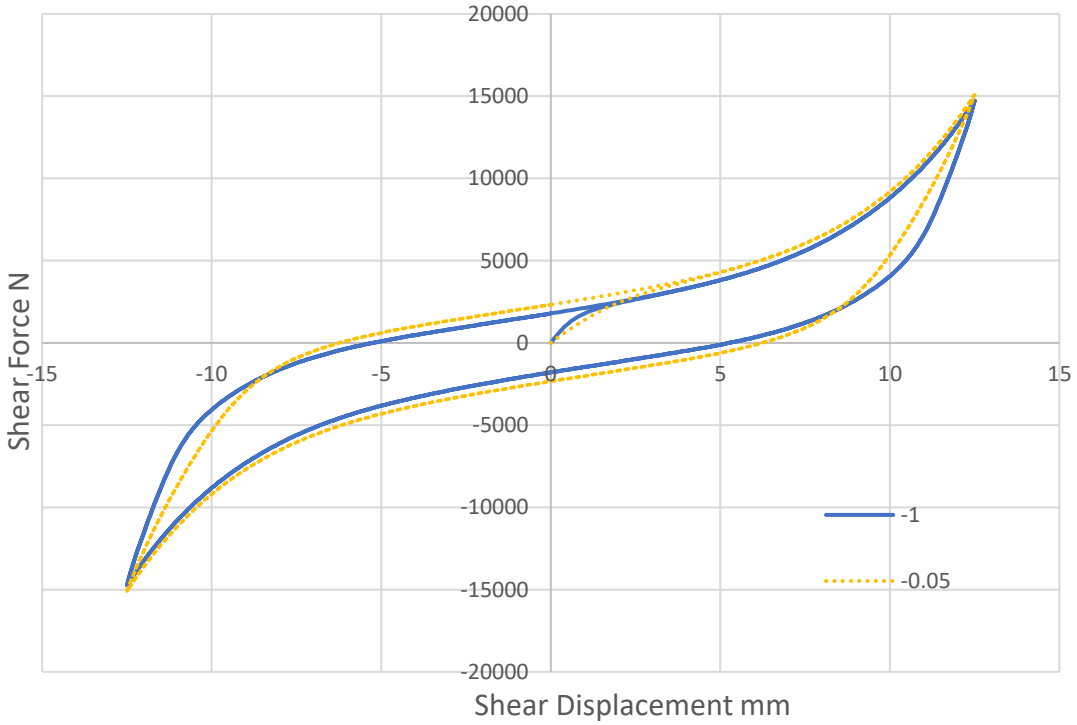

Figure 3.8. Creep strain factor sensitivity for models 1, 7.

Creep strain exponent effect is mainly observed during unloading. Elastomer tends to return to its original state faster with increasing value. This effect can be seen in Figure 3.8. Material shows slightly larger stress levels for increasing displacements.

3.1.2.5. Effective Creep Strain Rate (*E*). The creep strain rate close to the undeformed condition is regularized by this constant. Default value of ABAQUS (0.01) was used.

3.1.3. Material Model Validation

Main objective of this section is to check the validity of the material model for various loading rates.

A square geometry meshed with one element was used. Analyses are done with implicit time integration with nonlinear geometry assumption. The material is subjected to simple shear and compression loadings which are determined from industrial tests [3]. Loads are applied as displacements. Compression strain -0.5 and shear strain of 1 is applied.

For both compression and shear, all displacement boundary conditions are set to zero at bottom nodes (rotations and displacements in axis). For compression, horizontal displacement boundary conditions were set to zero and for shear, vertical displacement boundary condition was set to zero at top nodes.

3.2. Results

Predictions for simple shear and compression loadings are compared with the experimental values at different rates and validity of the model is discussed. Reaction forces and displacements in horizontal and vertical directions are used to calculate nominal stress and strain values, as well as vertical and horizontal stiffness.

Nominal compression stress is calculated by dividing the vertical reaction force to the undeformed cross-sectional area. Shear stress is calculated by dividing the horizontal reaction force to the undeformed cross-sectional area. Compressive strain is calculated as the ratio of decrease in height over the initial height of the rubber. Shear strain is the ratio of horizontal displacement to the thickness of the rubber. Vertical stiffness is the ratio of compressive nominal stress to the compressive strain at maximum displacement. Similar to vertical stiffness, horizontal stiffness is the ratio of shear stress to shear strain at maximum displacement.

3.2.1. Model Performance for Compressive Loading at Various Loading Rates

This section examines behavior of rubber material under compressive loads corresponding to -0.5 strain at various loading rates.

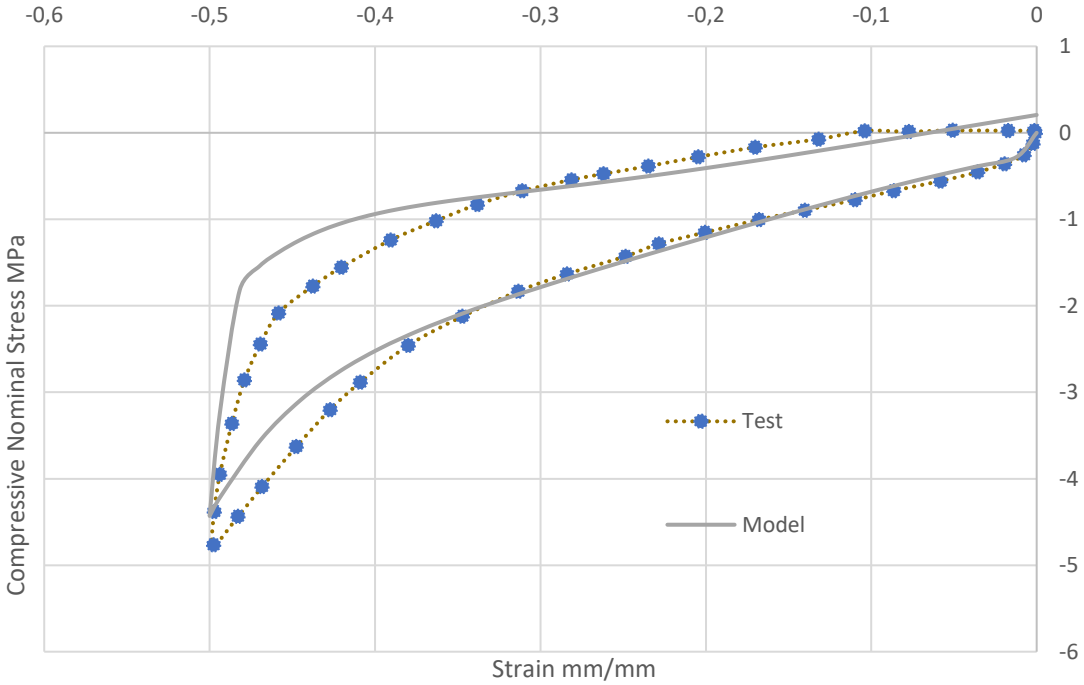

Figure 3.9. Uniaxial compression at 0.024/s strain rate [3].

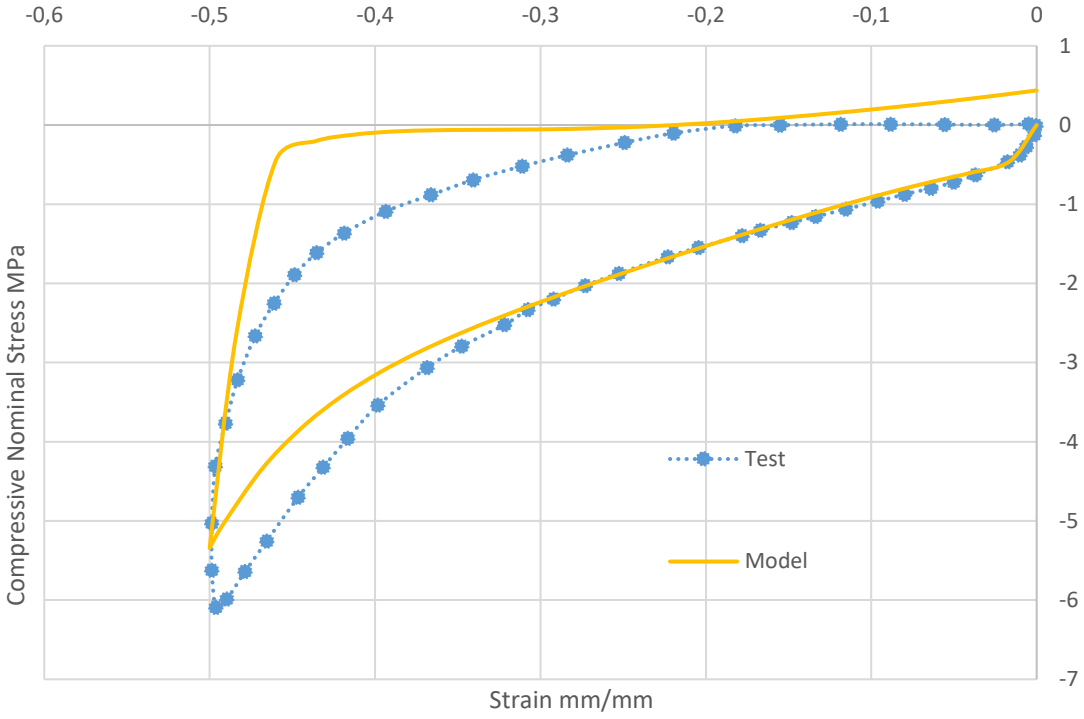

Figure 3.10. Uniaxial compression at 0.24/s strain rate [3].

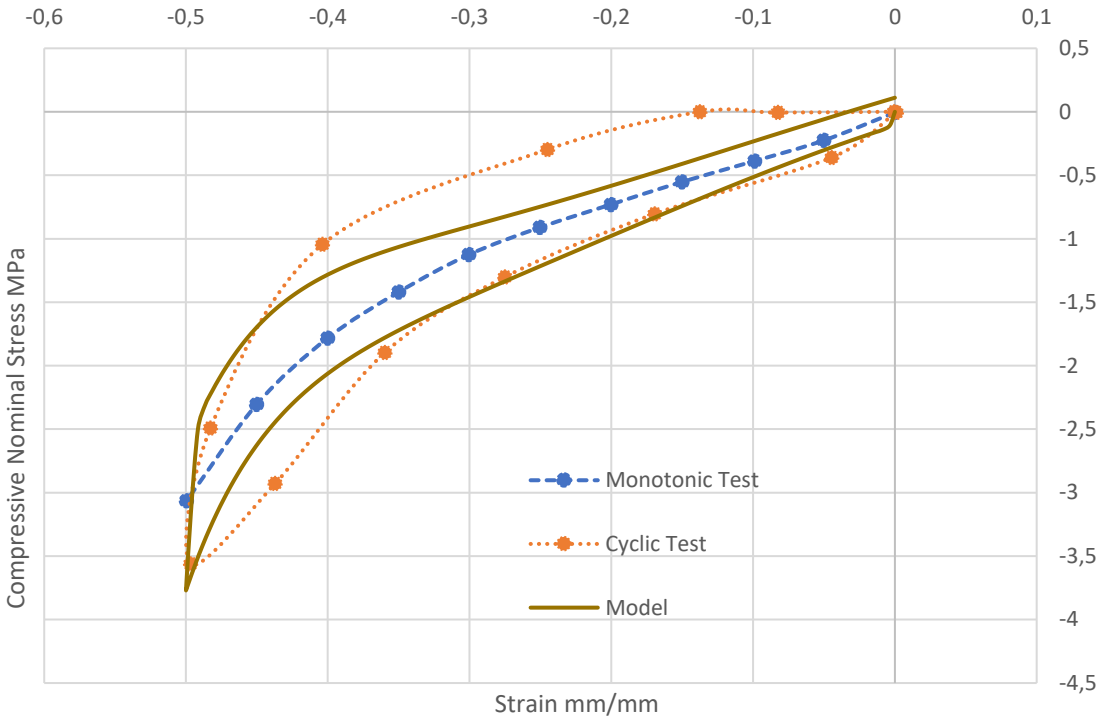

Figure 3.11. Uniaxial and cyclic compression results for 0.001/s strain rate [4].

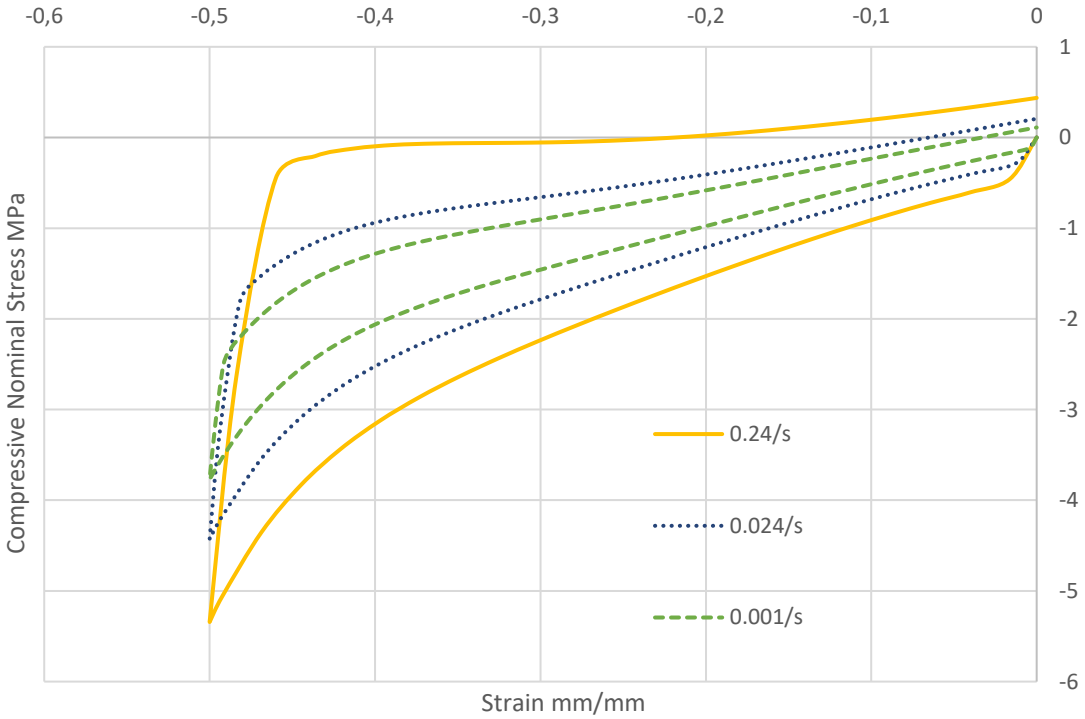

Figure 3.12. Model results for different strain rates.

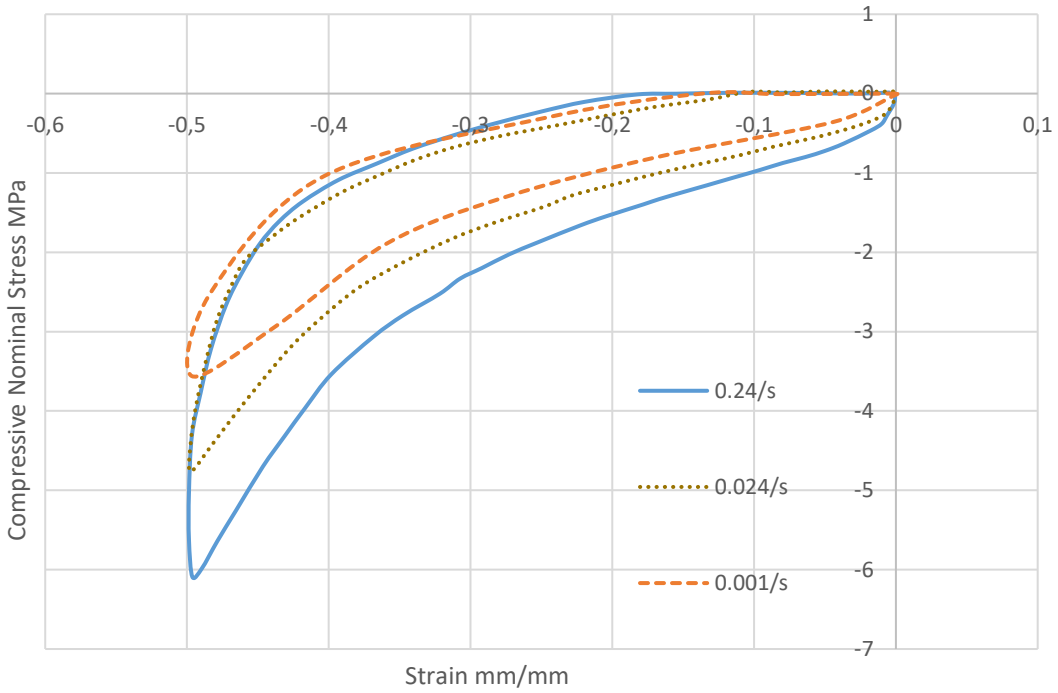

Figure 3.13. Test results for different strain rates [3].

Table 3.5. Comparison of cyclic uniaxial experiment and model results under different strain rates.

	Experiment		Model		
Strain Rate (/s)	Max Stress (MPa)	Stiffness (MPa)	Max Stress (MPa)	Stiffness (MPa)	Stiffness Error %
0.24	-6.09	12.28	-5.34	10.69	12.96
0.024	-4.76	9.57	-4.43	8.86	7.43
0.001	-3.56	7.17	-3.77	7.54	-5.21

Figures 3.9-3.13 show comparison between experimental and model values at different strain rates. Figure 3.12 shows model performance under various strain rates. Stress at maximum strain and stiffness values calculated from the predicted responses are given in Table 3.5. It is observed that higher loading rates result greater springback effects and sharper unloading curves. Lower strain rates show better agreement with data since Yeoh parameters were formed for equilibrium material behavior shown in Figure 3.11. The following conclusions can be made:

- Hysteresis hyperelastic model adds extra relaxation to unloading curve.
- Hysteresis hyperelastic model can model stiffness behavior of the material with 15 % error margin with one equilibrium test.
- Increase in strain rate results in higher stiffness values for experiments and model outputs.
- Maximum stress is underpredicted by 5-7 %.

3.2.2. Shear Loading

Shear loading predictions and their comparison with tests are reported in this section.

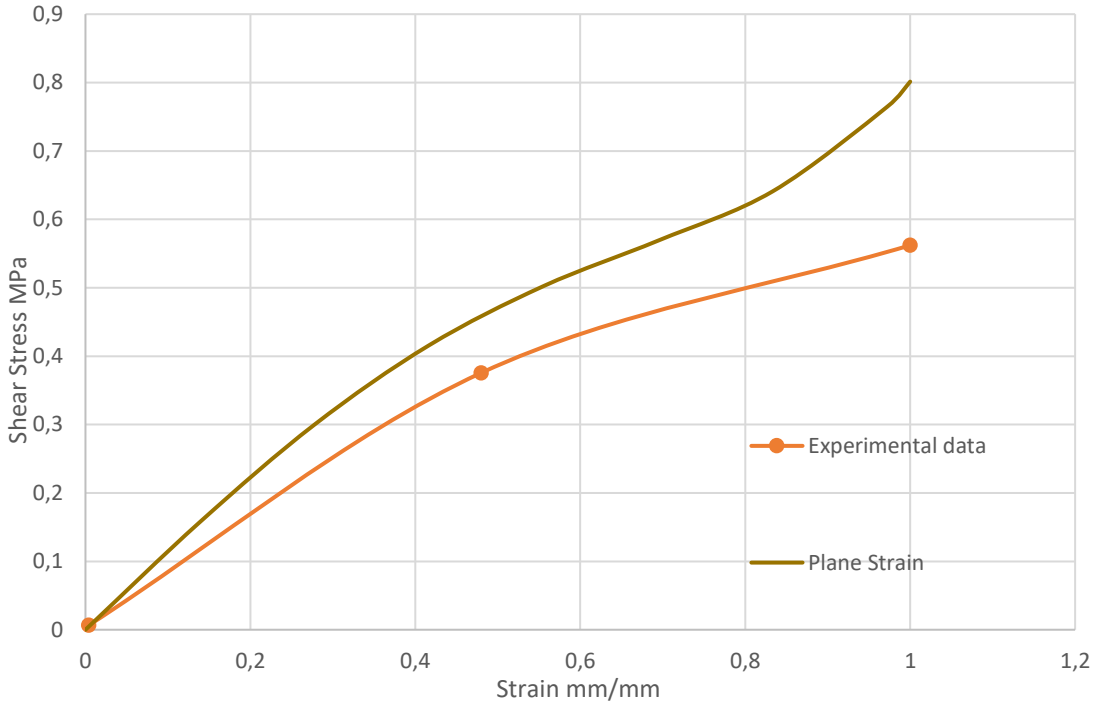

Figure 3.14. Model and experiment results for monotonic shear loading at strain rate 0.001/s [15].

Figure 3.14 shows the shear response for a monotonic loading at 0.001/s rate. The response is overpredicted by 29% at 100% shear strain. The difference in responses results from the fact that only compression test data was used in calibrating Yeoh model.

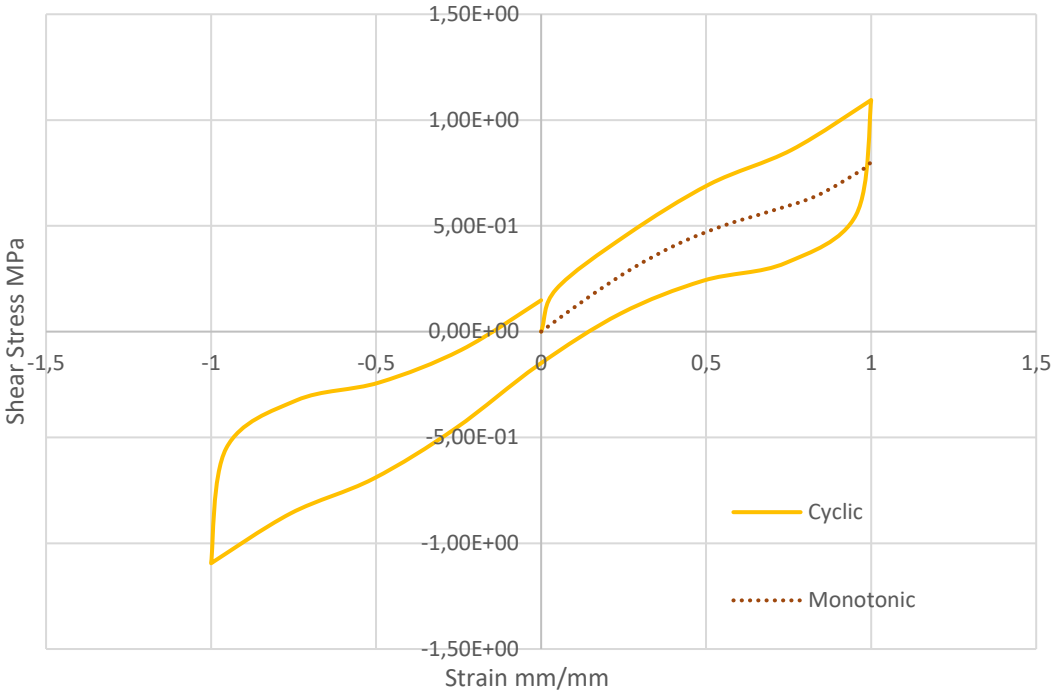

Figure 3.15. Hysteresis effect at strain rate 0.05/s.

Figure 3.15 compares monotonic and cyclic loading predictions. It is observed that hysteresis model adds slight stiffness to the response.

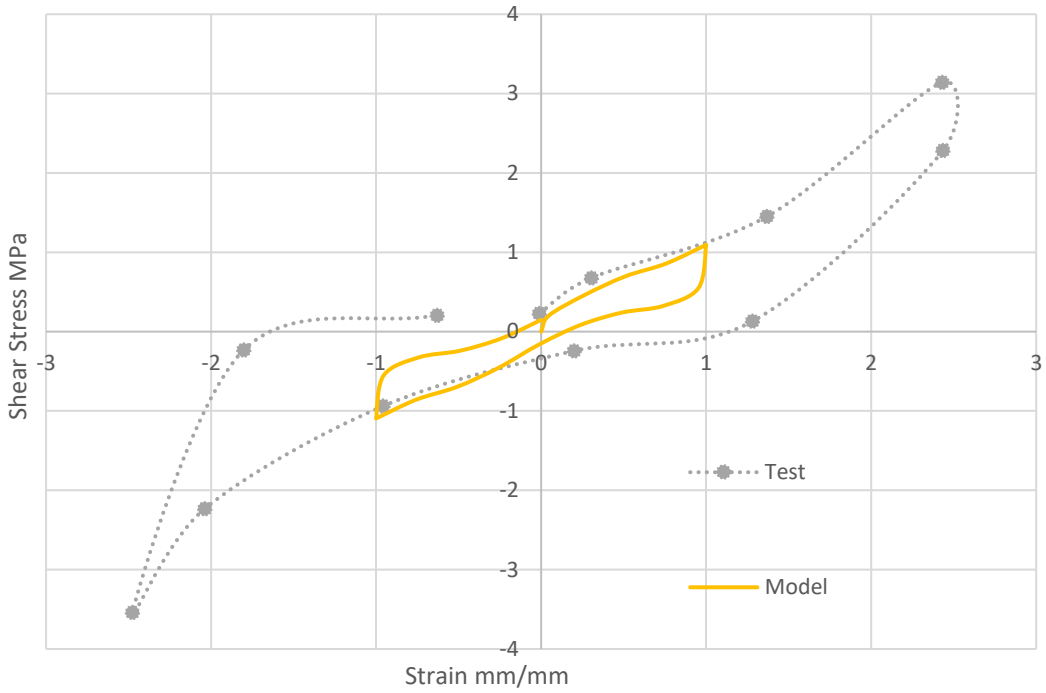

Figure 3.16. Simple shear at strain rate 0.05/s [3].

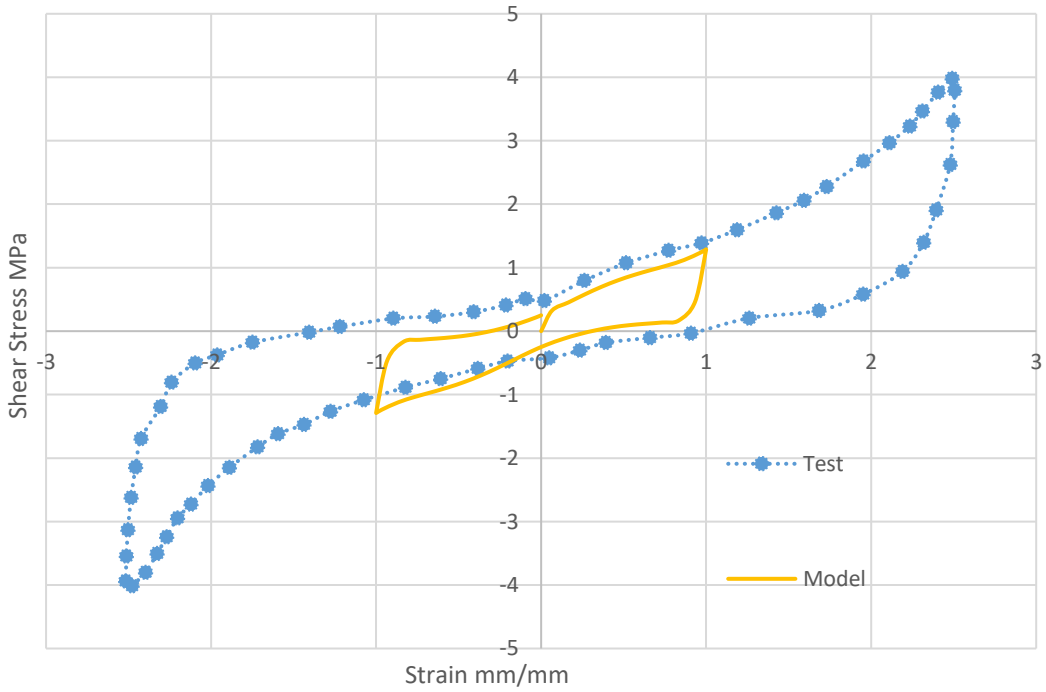

Figure 3.17. Simple shear at strain rate 0.4/s [3].

Table 3.6. Comparison of experiment and model stiffness for cyclic shear under different strain rates.

	Experiment		Model		
	Max Stress (MPa)	Stiffness (MPa)	Max Stress (MPa)	Stiffness (MPa)	Stiffness Error %
Cyclic Shear Test with Strain Rate 0.4/s	1.37	1.37	1.29	1.29	6.00
Cyclic Shear Test with Strain Rate 0.05/s	1.12	1.12	1.09	1.09	2.60

Test and model comparisons at two additional rates are shown in Figures 3.16 and 3.17 and the results are summarized in Table 3.6. Cyclic model calculates stress levels with high accuracy for slow and fast loadings. Lower rates of loading have slightly better accuracy.

Strain rate dependence of the response in shear loading is presented in Figure 3.18.

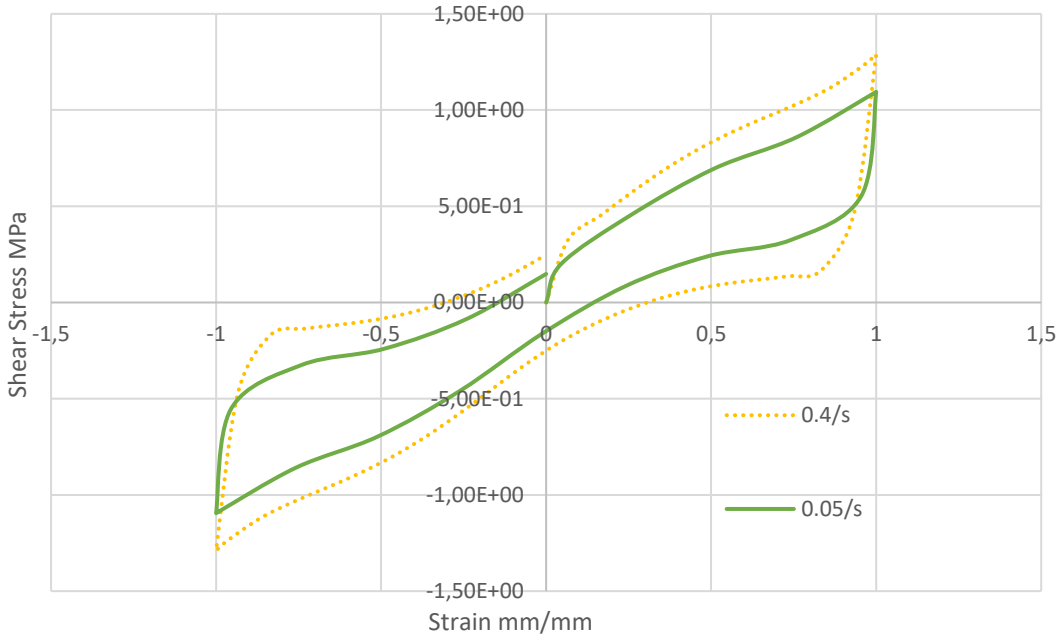

Figure 3.18. Model results for different strain rates.

The following conclusions can be made:

- Strain rate increase results in increased damping and stiffness as observed in experiments.
- Stiffness and maximum stress predictions agree well with test data.
- Dissipation predicted in cyclic loading is comparable to that observed in experiments.

3.3. Conclusions

Material model is calibrated using uniaxial compression test data at a single rate. Using the calibrated model shear and compression behavior of the high damping rubber is evaluated. Analysis results for compression of the HDR predicts stiffness and maximum stress values during cyclic loadings with less than 17% error margin. This margin diminishes to %2.5 in shear loads. Results from this section are used in bearing model.

- Hysteresis model implementation reasonably represents cyclic behavior of rubber.
- Hysteresis model results in higher relaxation at higher strain rates for compression.
- Hysteresis prediction in shear loading compares sufficiently well with data at low rates. Increasing loading rate results in higher deviations.
- As the loading rate rises, stiffness increases both for compression and simple shear.
- Loading rate increases the area between loading and unloading curves in cyclic loading so dissipated energy rises.

4. FINITE ELEMENT ANALYSIS OF COMPOSITE BEARING

Mechanical behavior of an elastomeric bearing with steel liners is investigated in this chapter. In order to obtain behavior of a high damping rubber bearing, a plane strain model is developed using ABAQUS software [10]. A small-scale rectangular bearing is selected for analysis. Hyperelastic and hysteresis model introduced in the previous chapter is used for HDR material. Analyses are obtained for compression and shear loadings. Sensitivity of results to changing compressibility, strain rate and mesh selection are examined. Reaction force and displacement output are used for calculation of stress-strain curves. Predictions are compared to test data when available.

4.1. Finite Element Model

This section presents details of material model, geometry, mesh properties, loading and analysis results of the bearing. The geometry of the bearing is given in Figure 4.1.

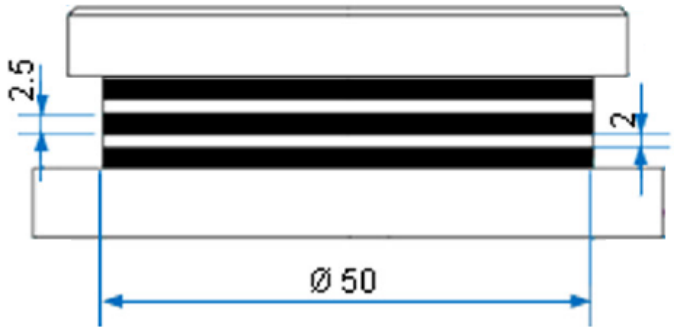

Figure 4.1. Drawing of the geometry.

4.1.1. Material Model

Material model used for HDR was described in Chapter 3. Both incompressible and compressible versions of this model are employed in this section.

The steel is represented by an elastoplastic material model with kinematic hardening [16]. Details of steel model are given in Table 4.1 and the uniaxial behavior is shown in Figure 4.2.

Table 4.1. Mechanical properties of steel.

Young Modulus E	200 GPa
Poisson's Ratio ν	0.3
Yield Stress σ_{yield}	276 MPa
Hardening Modulus E'	1034 MPa

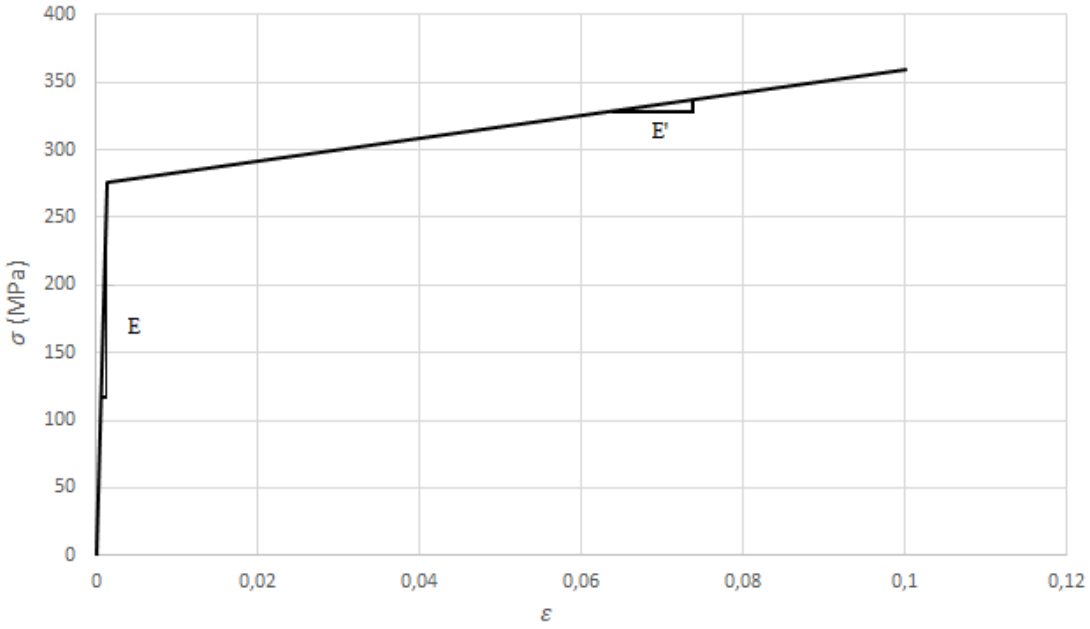

Figure 4.2. Stress-strain curve of steel.

4.1.2. Geometry of the Problem

A small bearing with shape factor of 5 and total bearing thickness of 11.5 mm is modelled [17]. Details of the geometry are given in Table 4.2 and the solid model is shown in Figure 4.3.

Table 4.2. Dimensions of HDRB.

Rubber Bearing Specifications	
Cross section	50 mm x 50 mm
Number of rubber layers	3
Number of steel layers	2
Thickness of each rubber layer	2.5 mm
Thickness of each steel layer	2 mm

Figure 4.3. Full bearing model.

4.1.3. Mesh

The following elements are used in the mesh.

- Rubber: CPE4RH. Bilinear, 4 noded plane strain element, reduced integration with hourglass control, hybrid with constant pressure.
- Steel: CPE4. 4 noded plane strain bilinear element.

4.1.4. Loading and Boundary Conditions

Compression and combined compression and shear loadings are considered. First, the bearing is analyzed under various compression strain rates. Then, the compression rate is kept constant and behavior at various shear strain rates are analyzed for combined loading.

Loads are applied as displacements through rigid surfaces which are placed at the top and bottom of the bearing. Top rigid surface is displaced according to compression and shear condition and bottom rigid surface is fixed.

Table 4.3. Vertical displacements for combined loading at different compressibility levels.

SF	Compressibility (κ_0/μ_O)	Compression Stress (MPa)	Vertical Displacement (mm)
5	∞	12	-0.17
	2000	12	-0.18
	100	12	-0.25
	10	12	-0.94

In the compression loading, bearing models with different compressibility levels are tested under 0.02 compression strain. For combined loading, compression stress is selected according to standard [18] where allowable compression stress is 12 MPa. Vertical displacements for this compression are given in Table 4.3. This table shows how much displacement is required for the bearing to reach 12 MPa of compression stress. Shear displacements are selected to simulate large seismic movements. In [18], strain magnitude 1 is recommended. Strain rates 0.05/s and 0.5/s are selected.

Interface conditions are defined between rubber, steel and rigid surfaces. Assumption of bounded bearing is made by the usage of tie constraint. This deduces two sides of the bearing being bounded to the top and bottom surfaces and horizontal rubber - steel interfaces. Tangential behavior is configured using the penalty friction formulation. The friction coefficient is selected to be $\mu = 0.3$.

Contact between sides of the bearing - rigid surfaces and sides of metal liners - rubber material is defined. Normal behavior is selected to be hard contact with Augmented Lagrange method.

4.2. Results

Finite element input and output used for characterization of the mechanical behavior of the bearing are listed as:

- Horizontal force,
- Horizontal displacement,
- Vertical displacement,
- Dissipated energy.

Based on the above predictions, the following properties are also calculated:

- Horizontal stiffness,
- Damping ratio.

Effects of the following parameters on bearing response and hysteresis loops are evaluated:

- Compressibility of rubber,
- Shear loading rate.

4.2.1. Compression Loading

Models are analyzed for slow and fast loading rates, 0.001/s and 0.24/s [3], respectively. Compressibility levels are selected to be 10, 100 and incompressible. Typically, rubber is modelled as incompressible. Compressibility 100 is a value suggested for explicit analysis. Compression level of 10 is used to determine the limit response of the model.

Compression stress is determined according to ISO 22762-2 where allowable compression stress is specified as 12 MPa. This stress corresponds to 30 kN force for the bearing considered in this study [19].

Deformed bearing geometry is shown in Figure 4.4 and compression loading predictions are given in Figure 4.5. Nominal stress is calculated by dividing reaction force to the undeformed cross-sectional area. Nominal strain is calculated as the ratio of the vertical displacement to the undeformed thickness of the bearing.

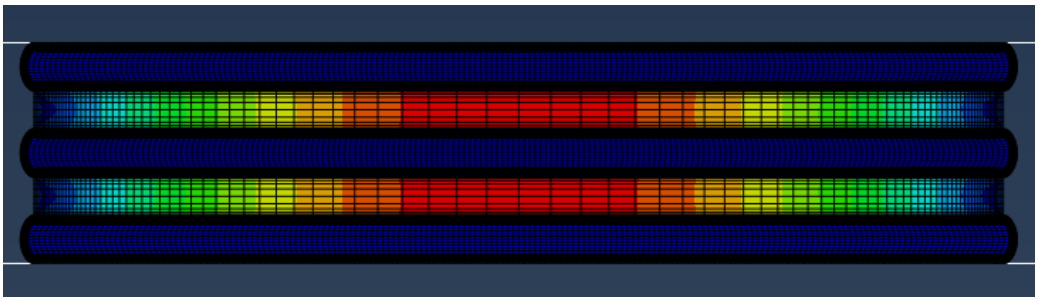

Figure 4.4. Deformed configuration of the bearing subjected to compression.

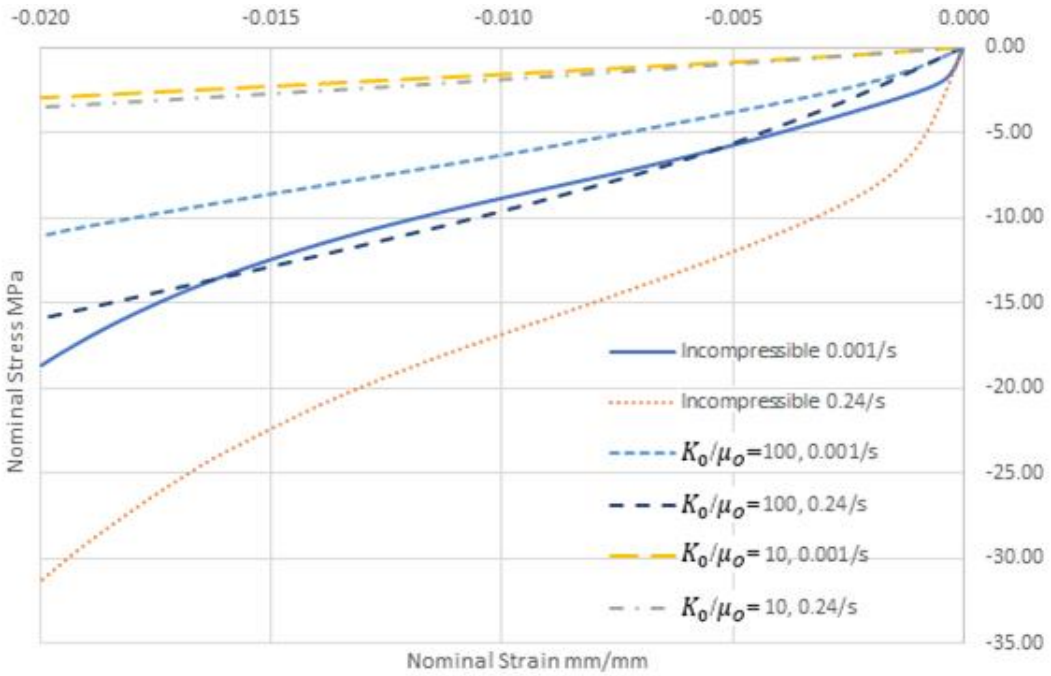

Figure 4.5. Compression loading at various compressibility values and strain rates.

4.2.1.1. Rate Effect on Compression Response. Rate effect on the vertical responses of HDRBs for different compressibility levels are shown in Figures 4.6-4.8. Results from these are compared in Table 4.4 by

$$\text{Stress Change} = \frac{\sigma_{fast} - \sigma_{slow}}{\sigma_{slow}}. \tag{4.1}$$

At all compressibility levels nominal compressive stress magnitude increases with increasing rates. As Table 4.4 shows, stress difference between slow and fast loading rates rises as the compressibility reduces. Incompressible bearing stress change is more than 3 times as compared to bearing with compressibility 10.

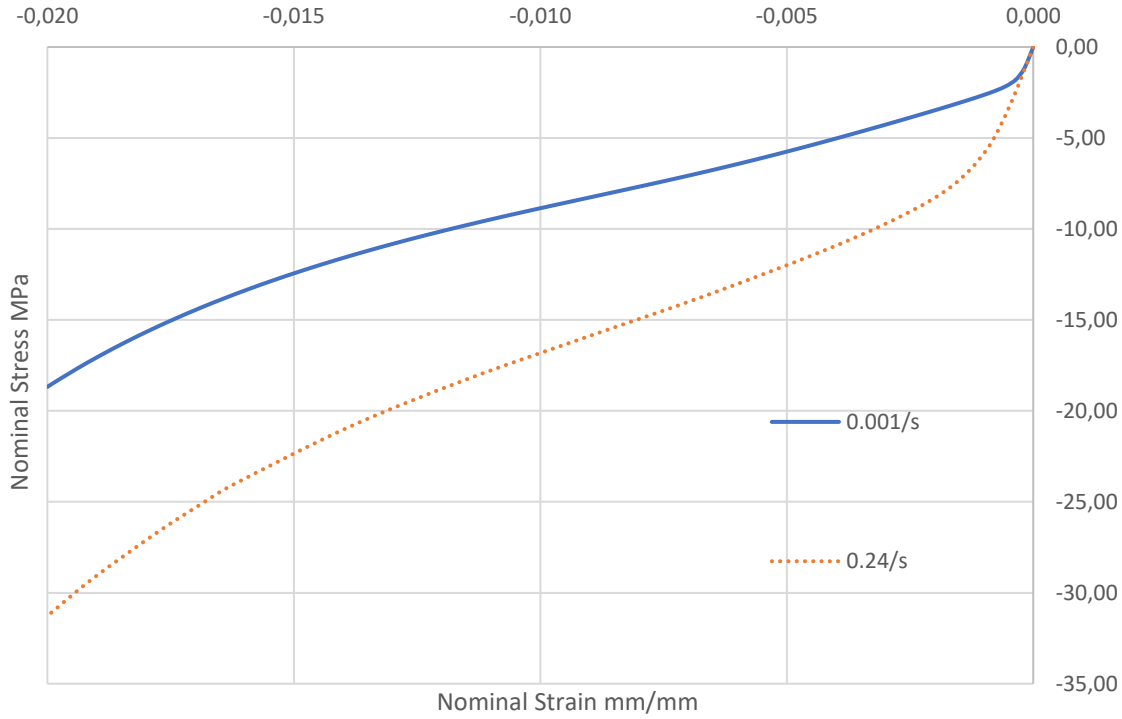

Figure 4.6. Compression loading for an incompressible model at various strain rates.

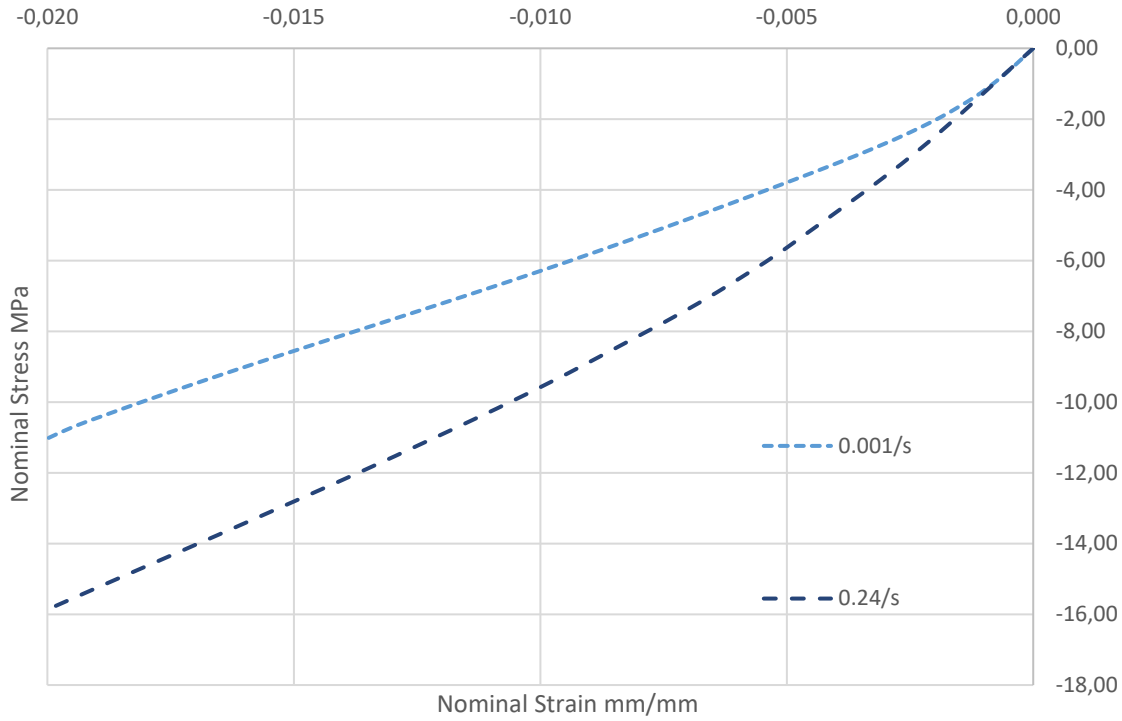

Figure 4.7. Compression loading for a compressibility 100 model at various strain rates.

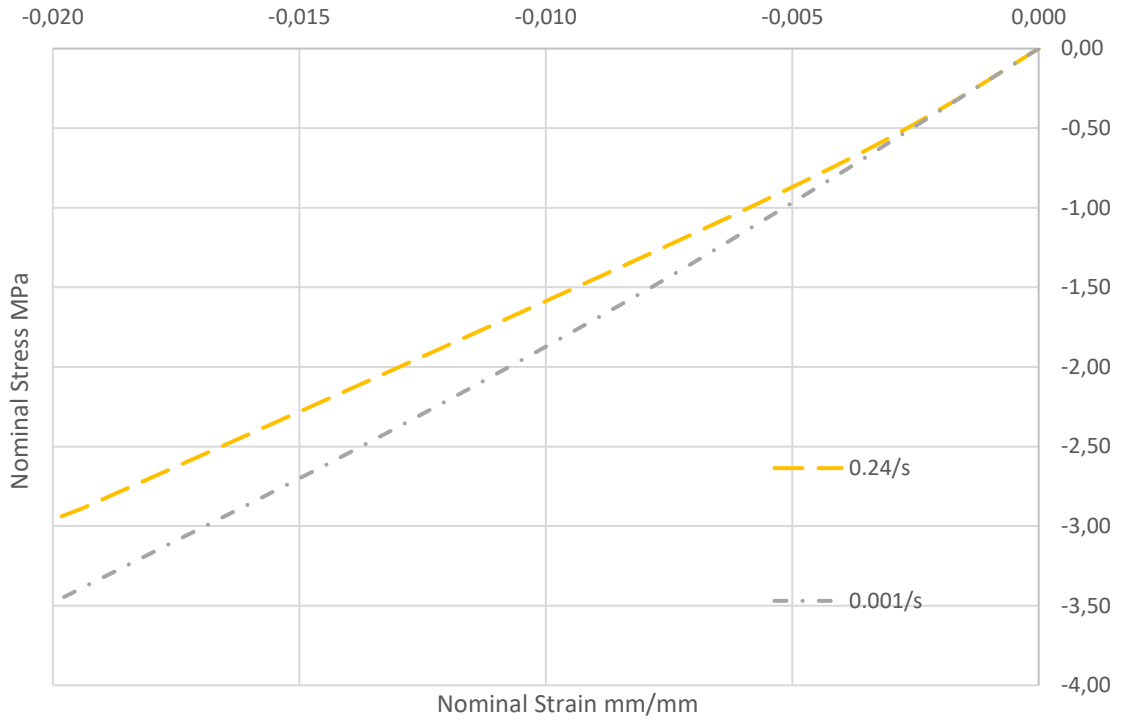

Figure 4.8. Compression loading for a compressibility 10 model at various strain rates.

Table 4.4. Stress change for compression at strain rates 0.001/s and 0.24/s for different compressibility levels.

Compressibility (K_0/μ_O)	Stress Change %
Incompressible	67.39
100	46.48
10	17.18

Observations on compressive loading can be summarized as:

- Loading rate have direct effect on bearing stiffness. As compression strain rate increases larger nominal stress levels are predicted.
- Depending on the compressibility level, stress change between two different strain rate loadings can reach up to 67 %.

4.2.1.2. Compressibility Effect on Compression Response. The effect of compressibility at slow and fast loading rates is given in Figures 4.9 and 4.10, respectively. Results from these are compared in Table 4.5 where the change of stress is calculated with respect to the incompressible model. Calculation formula is expressed as

$$\text{Stress Change} = \frac{\sigma_{compressible} - \sigma_{incompressible}}{\sigma_{incompressible}}. \qquad (4.2)$$

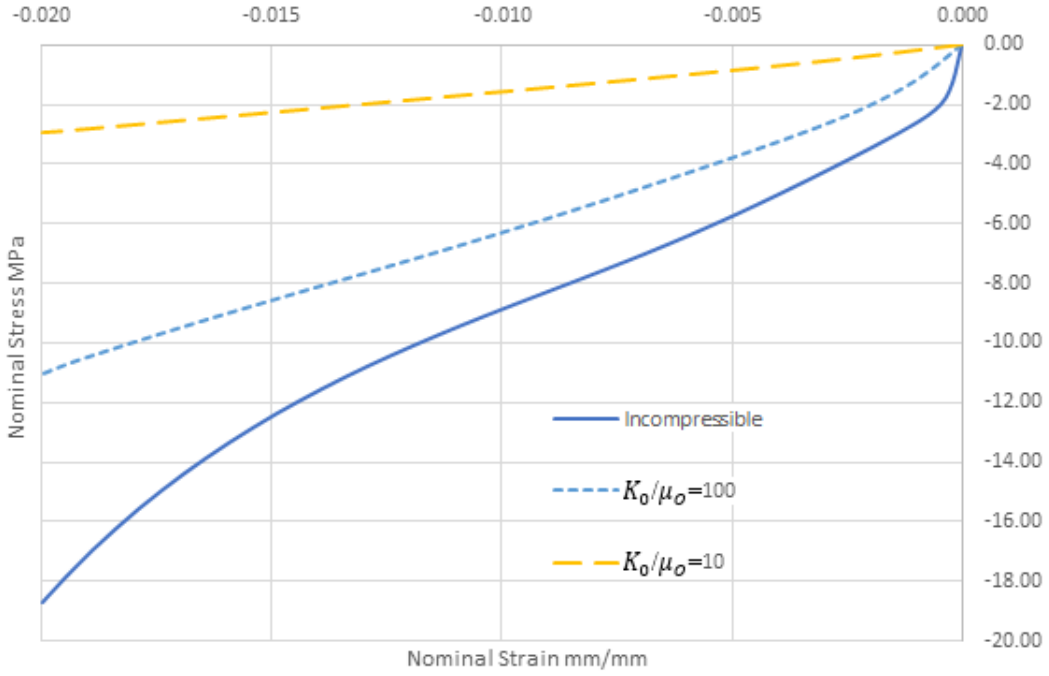

Figure 4.9. Compression loading at compression strain rate 0.001/s models with different compressibility values.

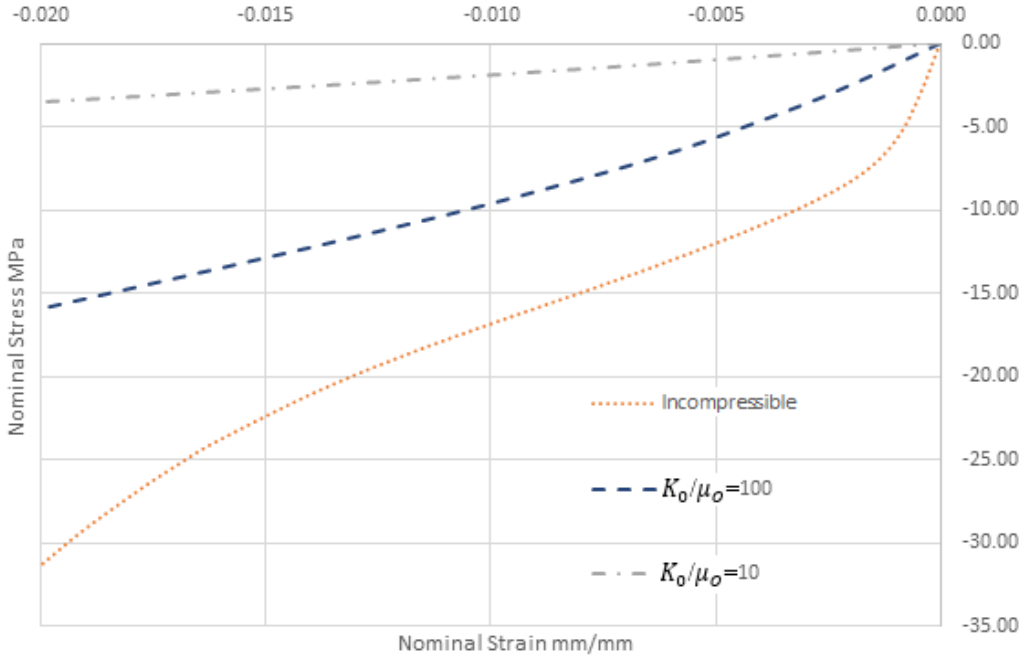

Figure 4.10. Compression loading at compression strain rate 0.24/s models with different compressibility values.

Table 4.5. Stress decrease at different compressibility levels with respect to the incompressible model.

	Compressibility	Stress Change %
0.001/s	100	-42.02
	10	-84.10
0.24/s	100	-49.26
	10	-88.87

According to Table 4.5 stress change for a given compressibility is similar at different loading rates, the difference being approximately within 5%.

Observations on compressibility effect in compression loading can be summarized as

- Reduction of compressibility results in increase in stiffness and stress.
- Increasing compressibility reduces stress change with respect to incompressible model prediction.
- Incompressible material has stronger stress dependence on the strain rate.

4.2.1.3. Hybrid Formulation Effect. Hybrid elements use a different formulation and are employed for nearly incompressible materials that is K_0/μ_O=2000 and K_0/μ_O=∞ require the use of hybrid elements, while standard elements are used in other K_0/μ_O values. In order to evaluate the effect of hybrid formulation, standard elements were used for K_0/μ_O=2000 and the predictions were compared.

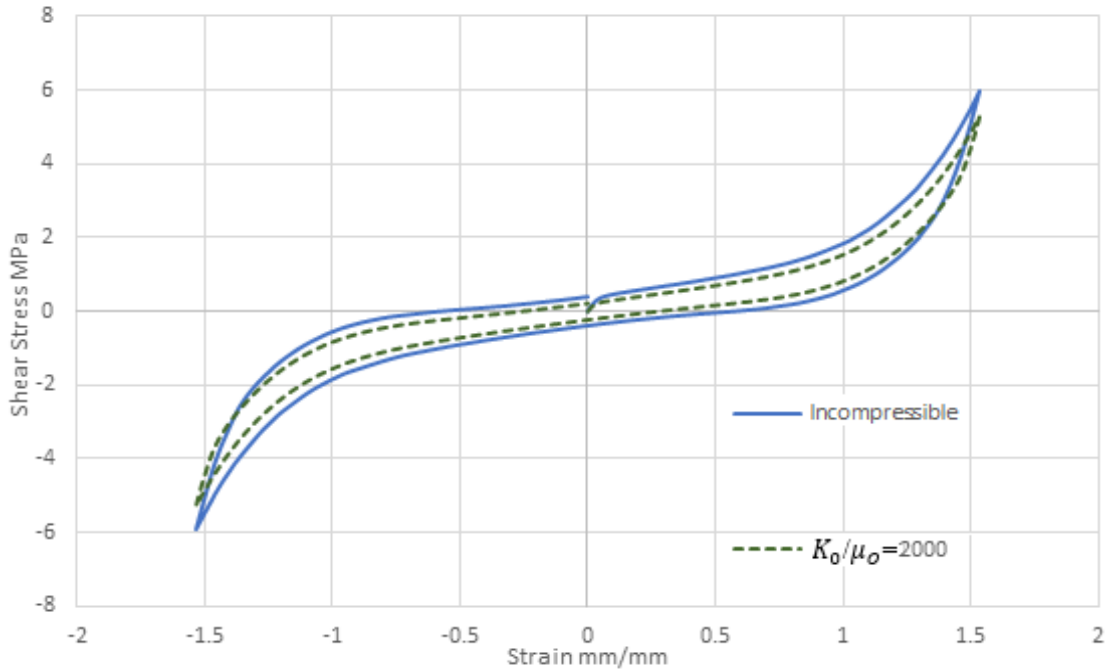

Figure 4.11. Comparison of incompressible and compressibility 2000 models for combined loading at strain rate 0.05/s.

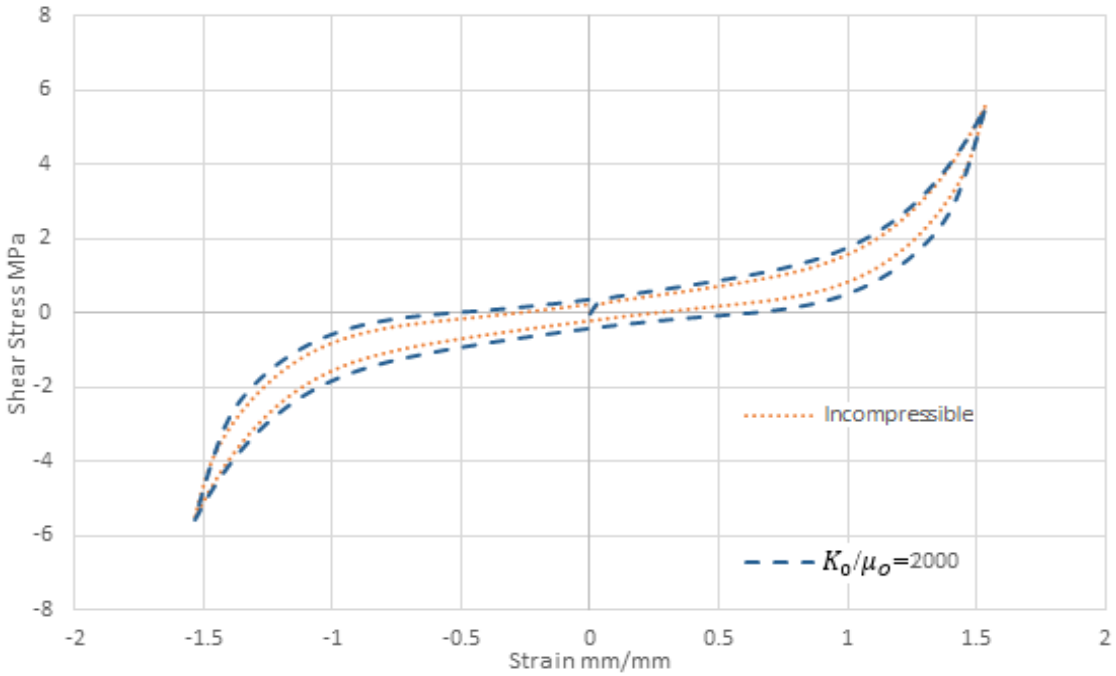

Figure 4.12. Comparison of incompressible and compressibility 2000 models for combined loading at strain rate 0.5/s.

Figures 4.11 and 4.12 clearly show that hybrid formulation does not alter the results and K_0/μ_O=2000 can be considered as incompressible.

4.2.2. Compression and Shear Loading

Rubber bearings are subjected to combined compression and shear loading. In particular 12 MPa compression is applied at 0.001/s rate and shear displacement of 11.5 mm corresponding to shear strain of 1.52 is applied to bearings. Figure 4.13 presents the deformed geometry of the bearing under compression and shear loading.

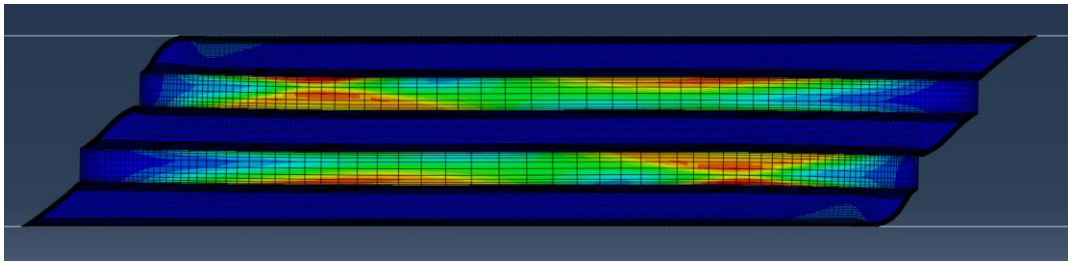

Figure 4.13. Deformed configuration of the bearing subjected to compression and shear loading.

In evaluating the bearing response, the dissipated energy is calculated as the area between reaction force-displacement hysteresis curve, shear modulus also known as shear stiffness, is calculated as the shear stress over shear strain at maximum displacement. Damping ratio is calculated as [17]

$$\zeta = \frac{2}{\pi} \cdot \frac{E_D}{K_{eff}(u_{max} - u_{min})^2} \tag{4.3}$$

where E_D represents the dissipated energy, K_{eff} is the slope of shear force-displacement curve at maximum strain and u are shear displacements. In the hysteretic material model used in this study E_D is the dissipated energy due to creep and is reported as ALLCD in ABAQUS.

4.2.2.1. Rate Effect on Combined Compression and Shear Response. Effect of shear strain rate on energy dissipation and shear stiffness are investigated. Rate effect on the horizontal response of HDRB for different compressibility levels are shown in Figures 4.14-4.16. Results are compared in Table 4.6.

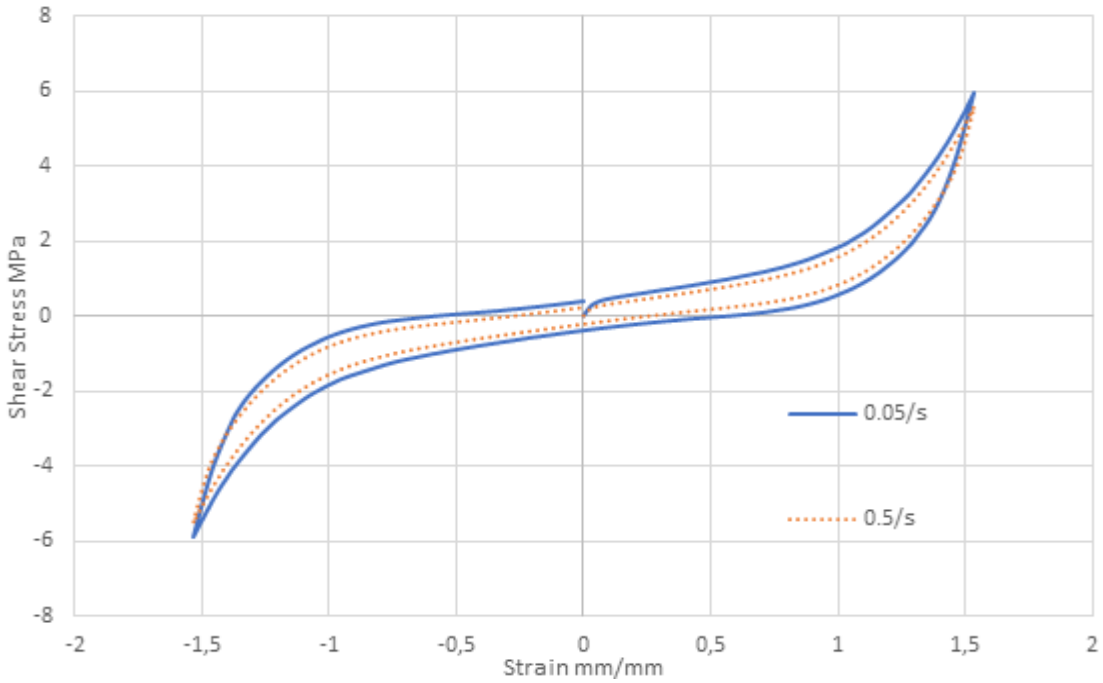

Figure 4.14. Combined loading response for incompressible model at different shear strain rates.

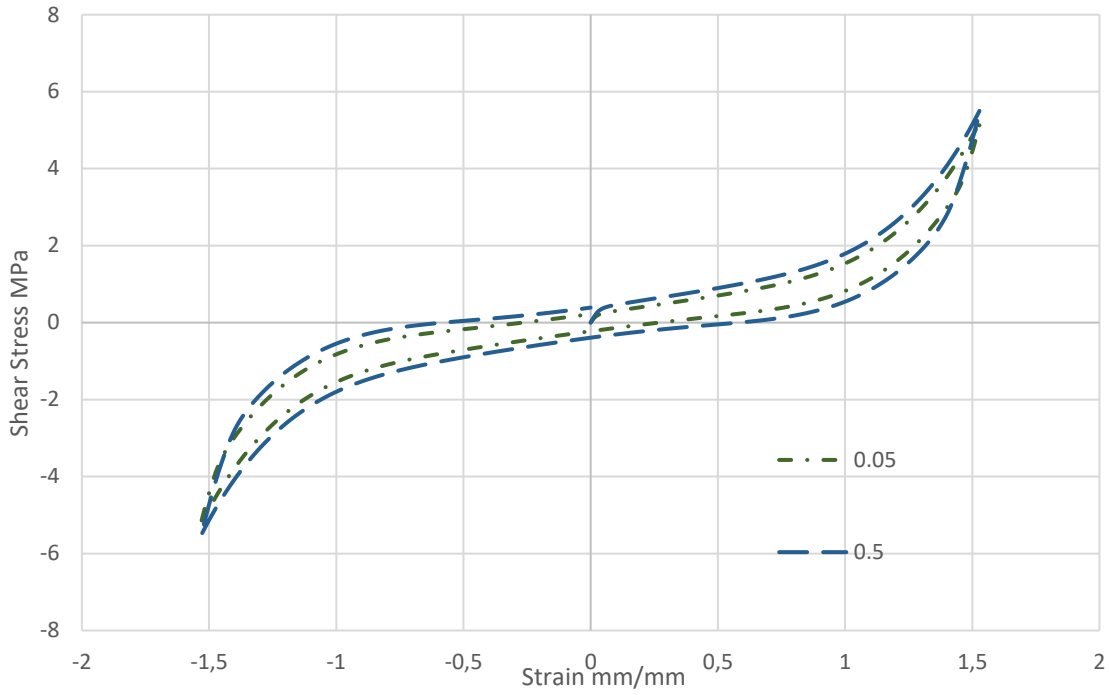

Figure 4.15. Combined loading response for K_0/μ_O=2000 model at different shear strain rates.

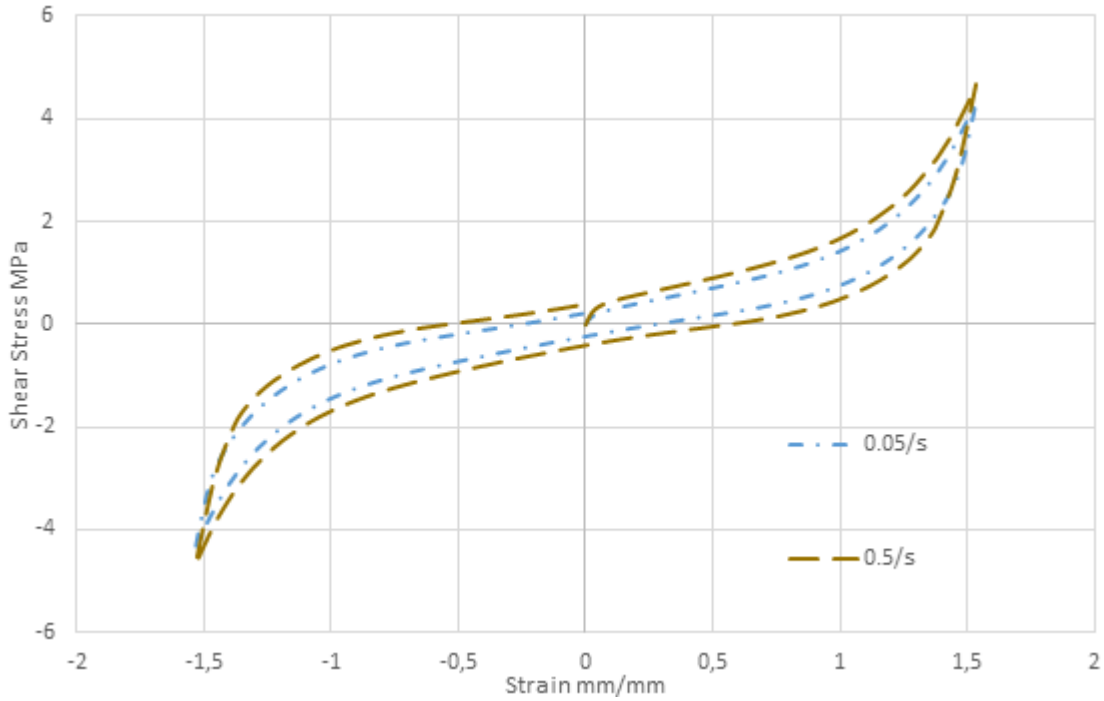

Figure 4.16. Combined loading response for K_0/μ_O=100 model at different shear rates.

In shear loading, faster loadings dissipate higher amounts of energy due to higher stress levels, therefore higher is the rate larger becomes the hysteresis, hence greater is the damping ratio. Loading rate also affects the shear stiffness, that is higher is the loading rate greater is the stiffness.

4.2.2.2. Compressibility effect on combined compression and shear response. Effect of compressibility values on energy dissipation and shear stiffness are investigated. The effect of compressibility is shown in Figures 4.17 and 4.18 for slow and fast loading rates, respectively.

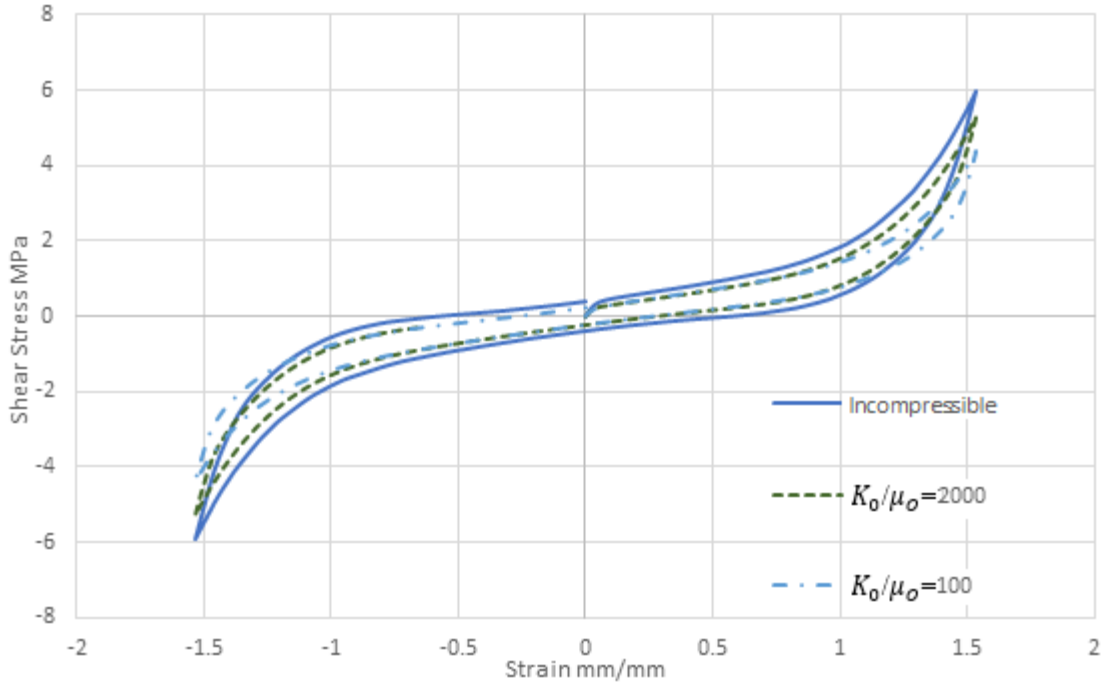

Figure 4.17. Combined loading response at shear strain rate 0.05/s for different compressibility levels.

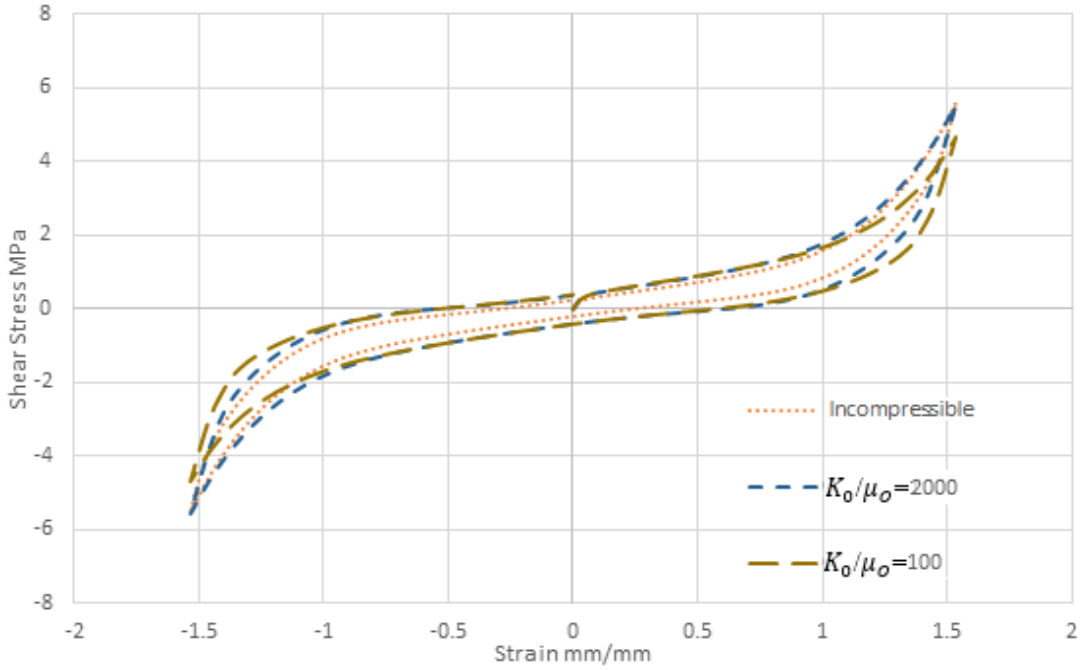

Figure 4.18. Combined loading response at shear strain rate 0.5/s for different compressibility levels.

Increasing compressibility results in shear modulus reduction and slight increase in damping ratio as seen in Table 4.6. [9,17] includes shear modulus between 1.9 to 2.94 and 1.52 to 2.1 respectively. Model results in Table 4.6 are on the stiffer side of these bearings.

Table 4.6. Bearing outputs under different compressibility and shear rate.

	Shear Strain Rate (1/s)	Dissipated Energy (N*mm)	Shear modulus (MPa)	Damping Ratio
Incompressible (Hybrid Element)	0.05	1.083E+05	3.64	0.107
	0.5	1.179E+05	3.88	0.11
Compressibility 2000	0.05	1.016E+05	3.43	0.107
	0.5	1.133E+05	3.62	0.113
Compressibility 100	0.05	8.600E+04	2.84	0.109
	0.5	9.814E+04	3.05	0.116

4.2.2.3. Comparison of predictions with experimental data. In [5], strain rate dependence of an HDRB is tested within a strain rate range of 0.05/s-5.5/s and maximum strain of 1.75. Results are shown in Figure 4.19. The experimental data are compared with model prediction in Figures 4.20 and 4.21, for slow and fast rates, respectively. Shear modulus and damping ratio are compared in Table 4.7.

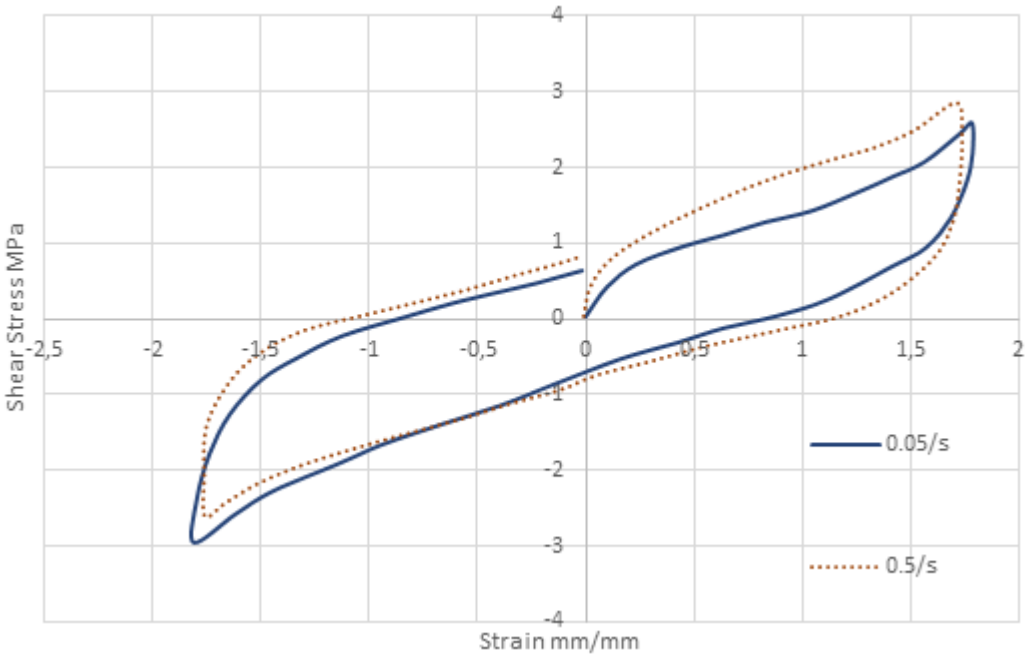

Figure 4.19. Combined loading experimental results for different shear strain rates [5].

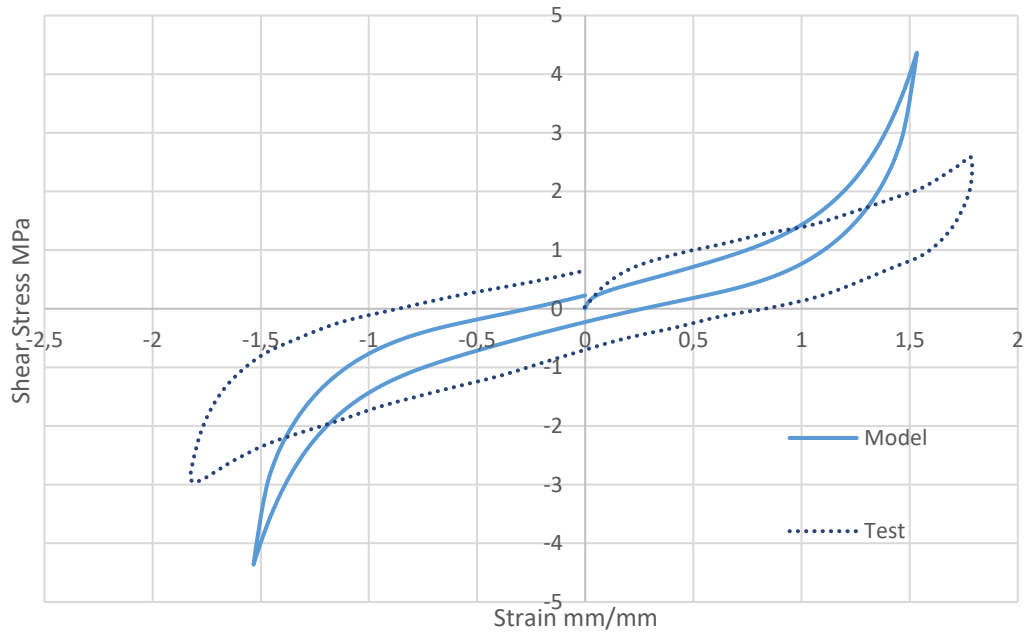

Figure 4.20. Combined loading comparison of model and experiment for shear strain rate of 0.05/s.

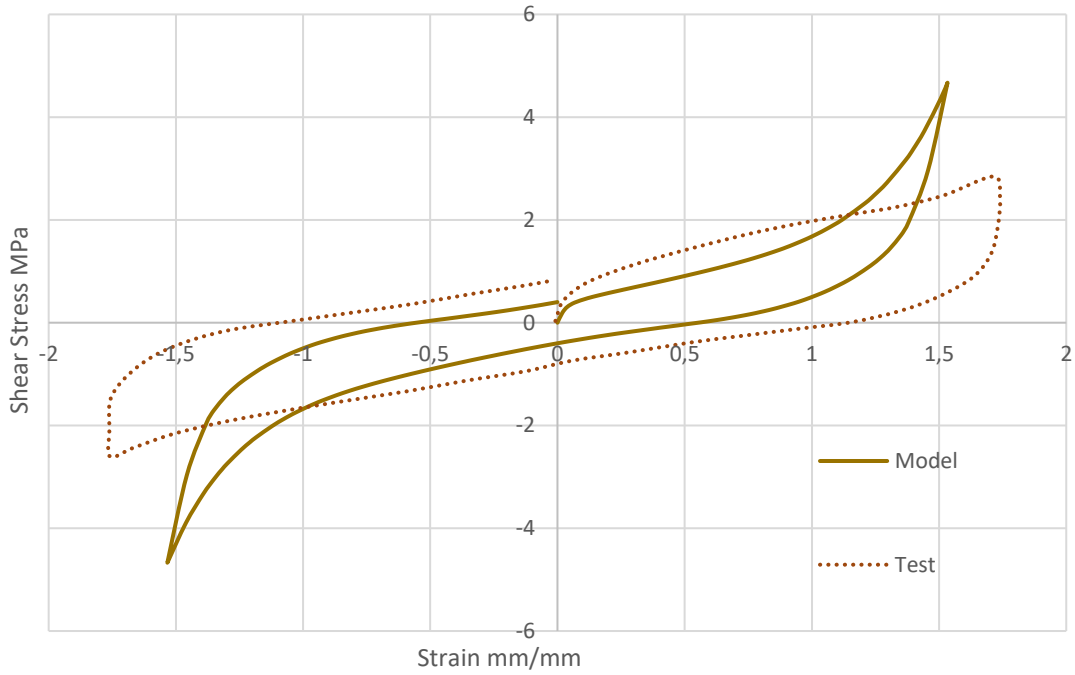

Figure 4.21. Combined loading comparison of model and experiment for shear strain rate of 0.5/s.

According to comparison between the model and test data, larger dissipation is observed in the experiments. Also, the stresses beyond strain of 1 are overpredicted. This may result from the fact that Yeoh model calibration is valid up to this value of shear strain. It may also be due to non-unique calibration of hysteresis model parameters.

Table 4.7. Comparison of model and experiment for different loading rates.

	Experiment		Model	
Shear Strain Rate (1/s)	Shear modulus (MPa)	Damping Ratio	Shear modulus (MPa)	Damping Ratio
0.05	1.45	0.16	2.85	0.09
0.5	1.63	0.19	3.05	0.116

High damping rubber bearings are shown to have damping ratio ranging from 0.10 to 0.23 [17], 0.1 to 0.28 in [20] and 0.16 to 0.22 in [9]. Predictions of this study are within the range reported in [9,20].

4.2.2.4. Hysteresis at multiple shear cycles. Figures 4.22-4.25 shows the response for three shear cycles at various rates and compressibilities. No difference in hysteresis is observed among loading cycles. Scragging effects are much more visible in softer bearings [10] and present in preliminary loads. Softening of the rubber material due to the Mullin's effect can be further added to the model.

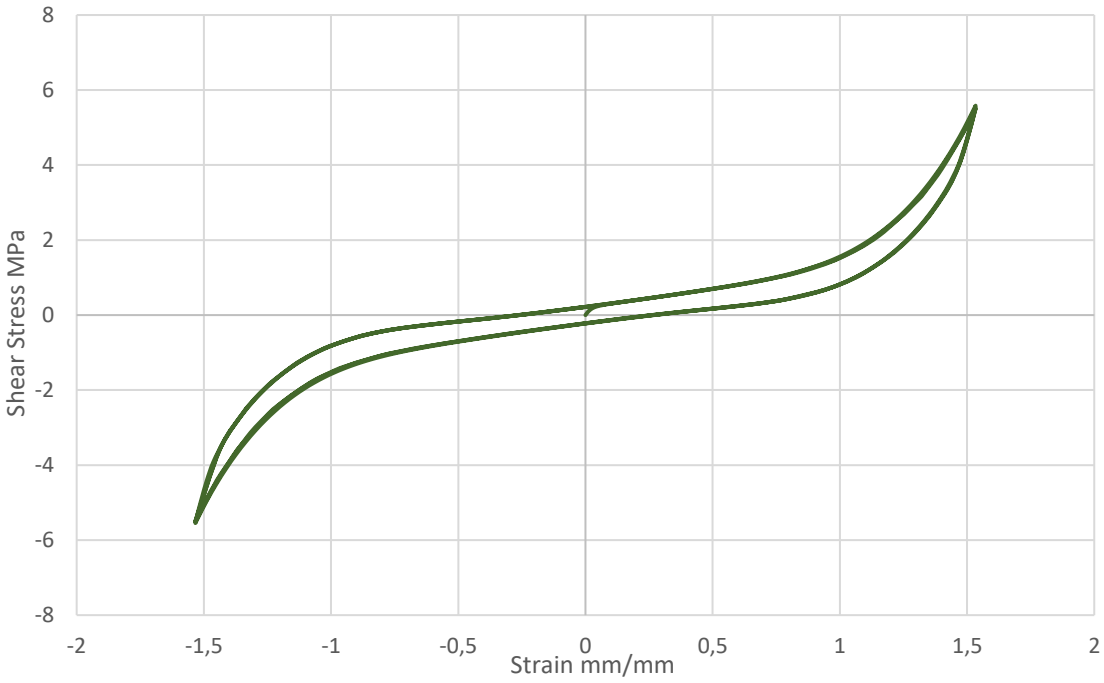

Figure 4.22. Combined compression and three cycles shear loading for incompressible model at shear strain rate 0.05/s.

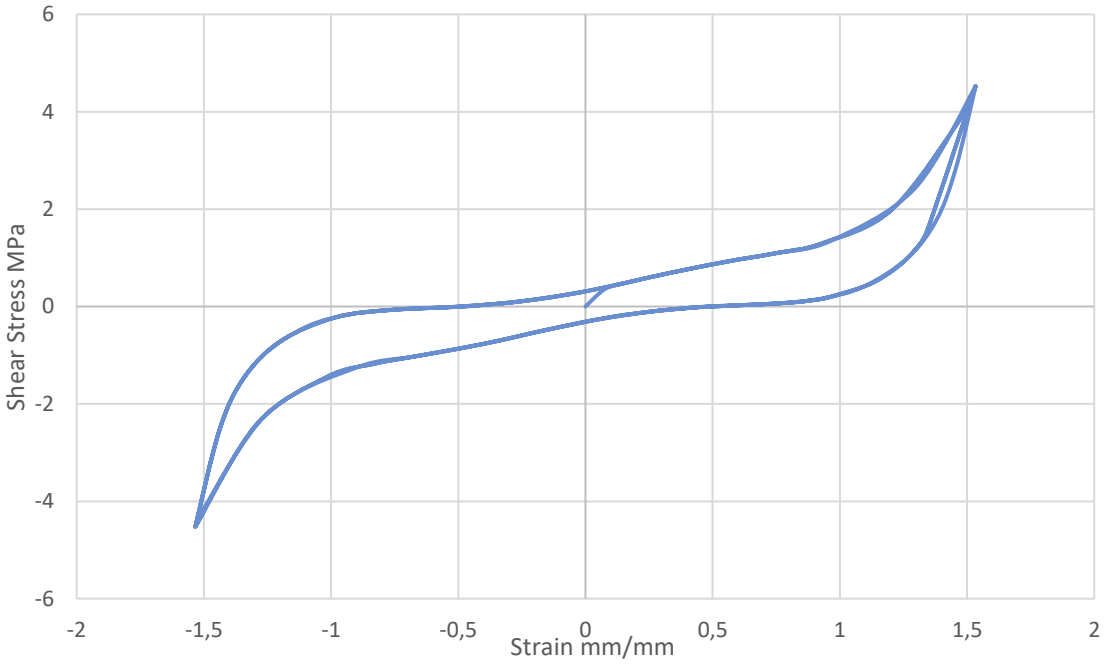

Figure 4.23. Combined compression and three cycles shear loading for incompressible model at shear strain rate 0.5/s.

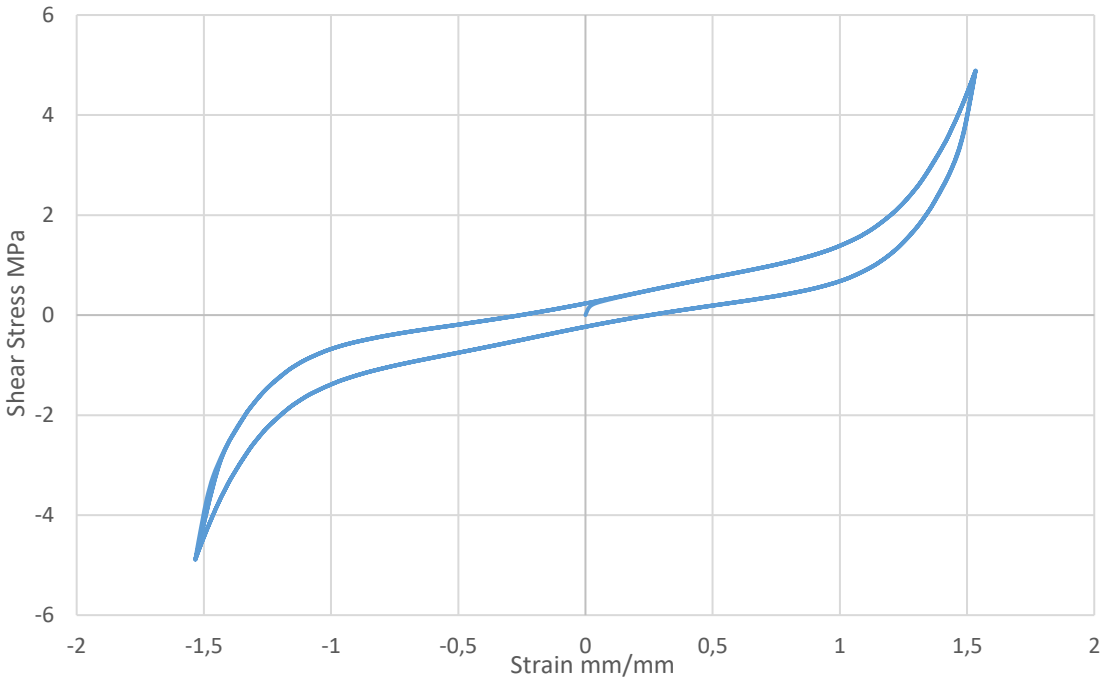

Figure 4.24. Combined compression and three cycles shear loading for K_0/μ_O=10 model at shear strain rate 0.05/s.

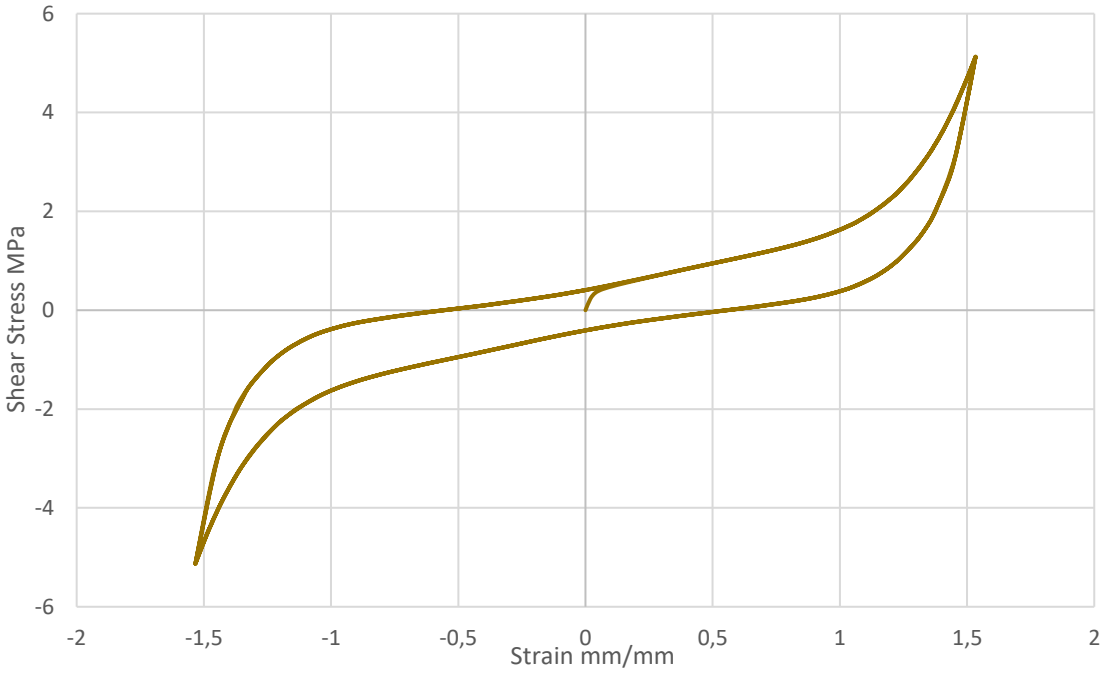

Figure 4.25. Combined compression and three cycles shear loading for K_0/μ_O=10 model at shear strain rate 0.5/s.

4.3. Conclusions

Based on the comparison of model prediction and experimental results the following points can be concluded:

- Higher loading rates increase nominal stress in compression.
- Increasing compressibility reduces the stress change with respect to incompressible model in compression.
- In compression, higher loading rate boosts stress difference with respect to incompressible model.
- Standard finite element formulation with compressibility level 2000 gives nearly the same results as the hybrid element formulation.
- In shear loading, stiffness and dissipated energy are directly proportional to the loading rate.
- Increase in compressibility results in reduction of shear modulus and increase in damping ratio.

5. FINITE ELEMENT ANALYSIS OF AN INDUSTRIAL BEARING

Small scale bearing with shape factor 5 was analyzed in Chapter 4. In this chapter, a full-size industrial bearing with factor 12 is investigated. Particular bearing geometry from [4] is selected due to detailed experimental tests available for comparison.

The effects of the compressibility and strain rate on the bearing response are investigated.

5.1. Finite Element Model

A computational strategy for large strain, hyperelastic model with hysteresis is developed and analyzed for HDRB under compression and shear loading.

5.1.1. Material Model

High damping rubber material model developed in Chapter 3 was used. Steel liners between rubber layers were represented with the elastoplastic model given in Chapter 3.

5.1.2. Geometry of the Problem

A mid-sized industrial bearing with metal liners and shape factor of 12 is modelled. Overall thickness is 41.5 mm and further details are given in the Table 5.1. Solid model is shown in Figure 5.1.

Table 5.1. Geometry data of HDRB [4].

Rubber Bearing Specifications	
Cross section	240 mm x 240 mm
Number of rubber layers	6
Number of steel layers	5
Thickness of each rubber layer	5 mm
Thickness of each steel layer	2.3 mm

Figure 5.1. Full-size bearing model.

5.1.3. Mesh

Mesh size is selected based on [4] and is shown in Figure 5.2. The mesh convergence study is presented in Appendix-A.

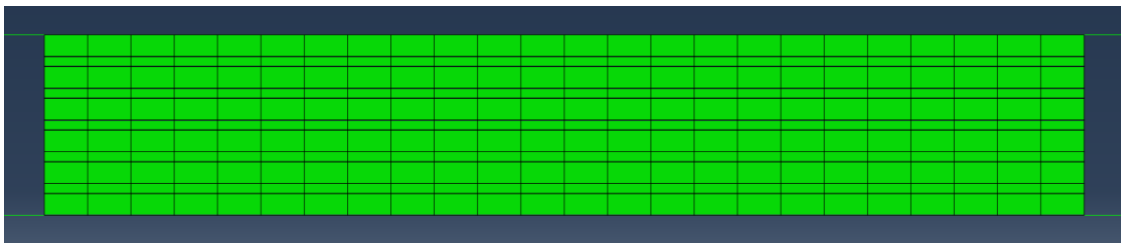

Figure 5.2. Full-size bearing model mesh.

The following elements are used in the mesh.

- Rubber: CPE4RH. Bilinear element, reduced integration with hourglass control, hybrid with constant pressure.
- Steel: CPE4. 4 node bilinear element.

5.1.4. Loading and Boundary Conditions

The applied load was selected to correspond to average compression stresses of 6 MPa [4] and 12 MPa [18] to allow determining the dependence of the shear response on compression load. The shear strain was applied as 1.42, larger than the previously applied value of 1.

All displacement boundary conditions are set to zero at bottom nodes as shown in Figure 5.3. First, compression load was applied. This was followed by shear displacement applied to top surface. Compression strain rate was selected to be 0.001/s [4]. Two shear strain rates were selected as 0.05/s and 1.5/s [4].

Contact and interface conditions were the same as those used in the model described in Chapter 4.

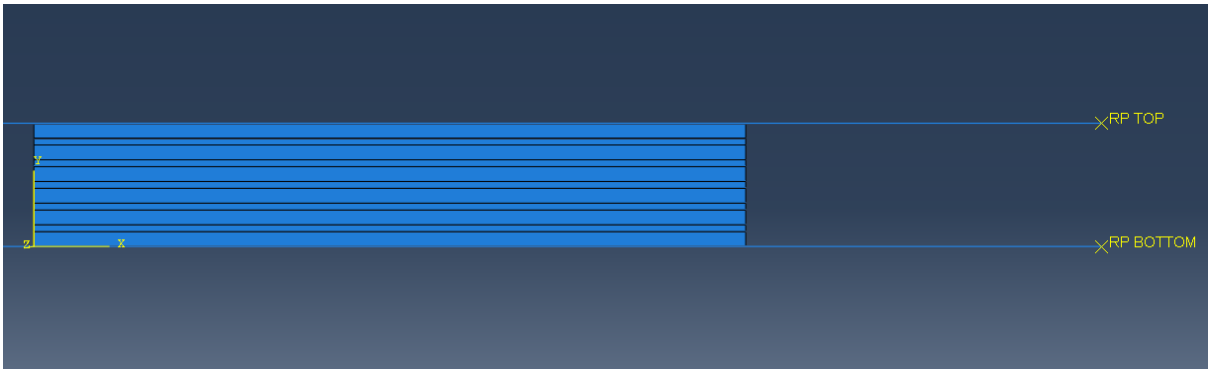

Figure 5.3. Full-scale bearing model boundary conditions.

5.2. Results

Deformed configuration of the bearing is shown in Figure 5.4. Mechanical response of the bearing was evaluated based on the following outputs:

- Horizontal force and displacement,

- Vertical load and displacement,
- Dissipated energy.

The effect of the following properties on the bearing response for combined compression and shear loading were investigated:

- Compressibility of rubber,
- Compression load magnitude,
- Shear loading rate.

The available test data [4] is for monotonic loading, while the prediction was done for cyclic loading. The comparison is given in Figure 5.5. Close correlation between model and experiment validates the developed material model. The model can be, therefore, used to obtain response for other loadings without running multiple tests.

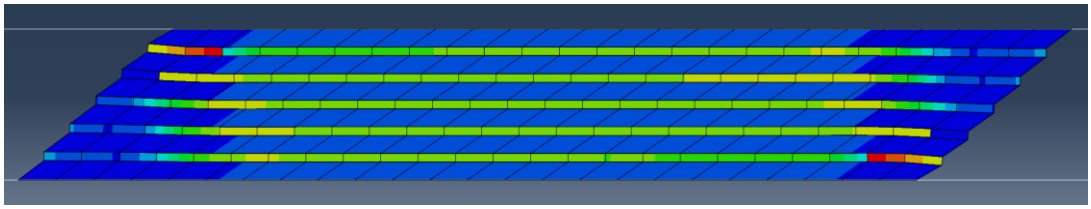

Figure 5.4. Meshed model for the deformed shape.

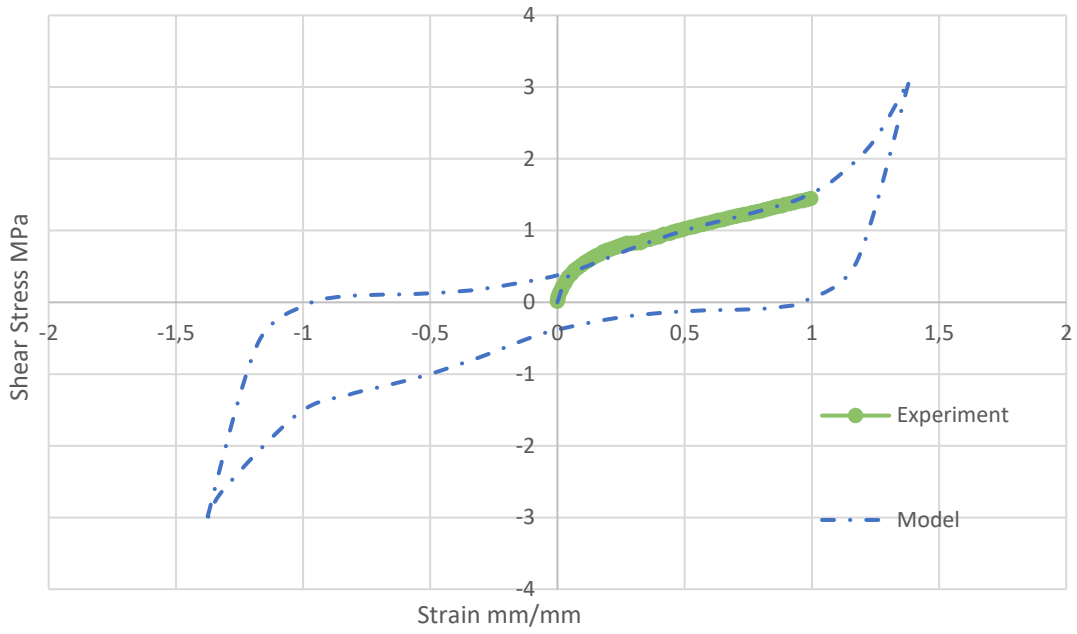

Figure 5.5. Experimental and model data comparison for shear strain rate of 1.5/s [4].

5.2.1. Compressibility Effect

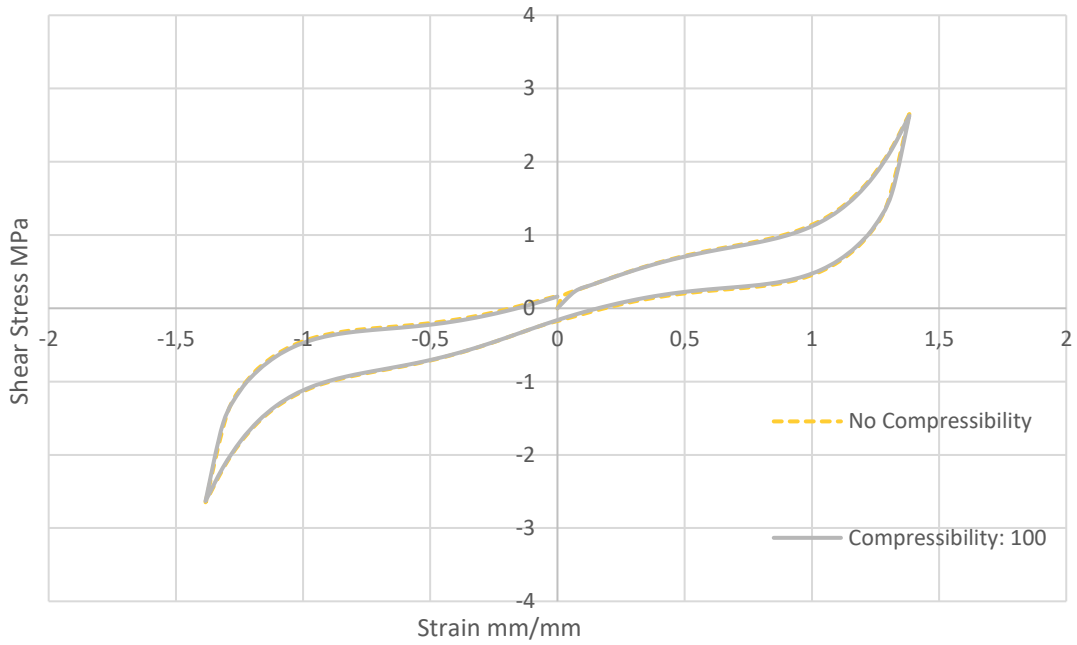

Figure 5.6. Shear strain rate 0.05/s models with different compressibility.

Response of HDRB are shown in Figure 5.6 and Table 5.2 at different compressibility levels. The quantities in Table 5.2 were calculated as described in section 4.2.2.

Reduction of compressibility results in slightly greater damping and shear modulus.

Table 5.2. Comparison between compressibility levels.

Compressibility (m^2/N)	Dissipated Energy (N*mm)	Shear modulus (MPa)	Damping Ratio
Incompressible	4.92E+06	1.894	0.124
Compressibility 100	4.82E+06	1.880	0.122

5.2.2. Compression Load Effect

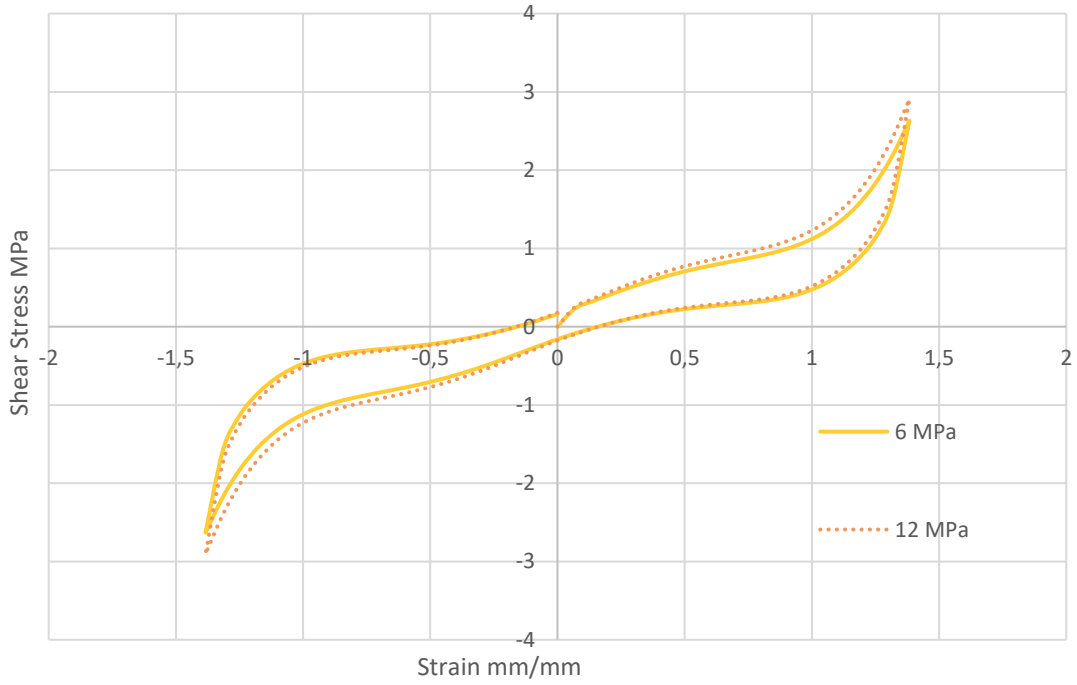

Figure 5.7. Shear strain rate 0.05/s and compressibility 100 model with different compression magnitudes.

Compression load on the bearing is due to structure, seismic device or machinery weight. To evaluate the effect of load magnitude, 6 MPa and 12 MPa were analyzed. Shear loads on the bearing are kept constant in terms of magnitude and rate so dependence on vertical load is studied. The results are compared in Figure 5.7, Table 5.3 and show that wedging the bearing with larger loads results in higher dissipated energy and stiffness levels.

Table 5.3. Compression load effect.

Compressive Stress (MPa)	Dissipated Energy (N*mm)	Shear modulus (MPa)	Damping Ratio
6	4.82E+06	1.880	0.122
12	5.32E+06	2.075	0.134

5.2.3. Shear Strain Rate Effect

Analysis results at slow and fast shear strain rates are shown in Figures 5.8, 5.9, Tables 5.4 and 5.5. Overall, shear strain rate has a considerable effect on the calculated values, for all compressibility levels. This conclusion is in agreement with literature [21].

Shear modulus and damping ratio dependence on strain rate is larger for incompressible material. Damping ratio of the incompressible material increases by 15 % for 1.5/s shear strain rate in comparison to strain rate of 0.05/s. The difference is reduced to 7.5 % for higher compressibility. Shear modulus increase for incompressible case is 14.4 % and 9.2 % for higher compressibility.

Table 5.4. Shear strain rate effect for incompressible material.

Shear Strain Rate (1/s)	Dissipated Energy (N*mm)	Shear modulus (MPa)	Damping Ratio
0.05	4.92E+06	1.894	0.124
1.5	6.84E+06	2.213	0.147

Table 5.5. Shear strain rate effect for compressibility 100.

Shear Strain Rate (1/s)	Dissipated Energy (N*mm)	Shear modulus (MPa)	Damping Ratio
0.05	4.82E+06	1.880	0.122
0.5	5.78E+06	2.077	0.132

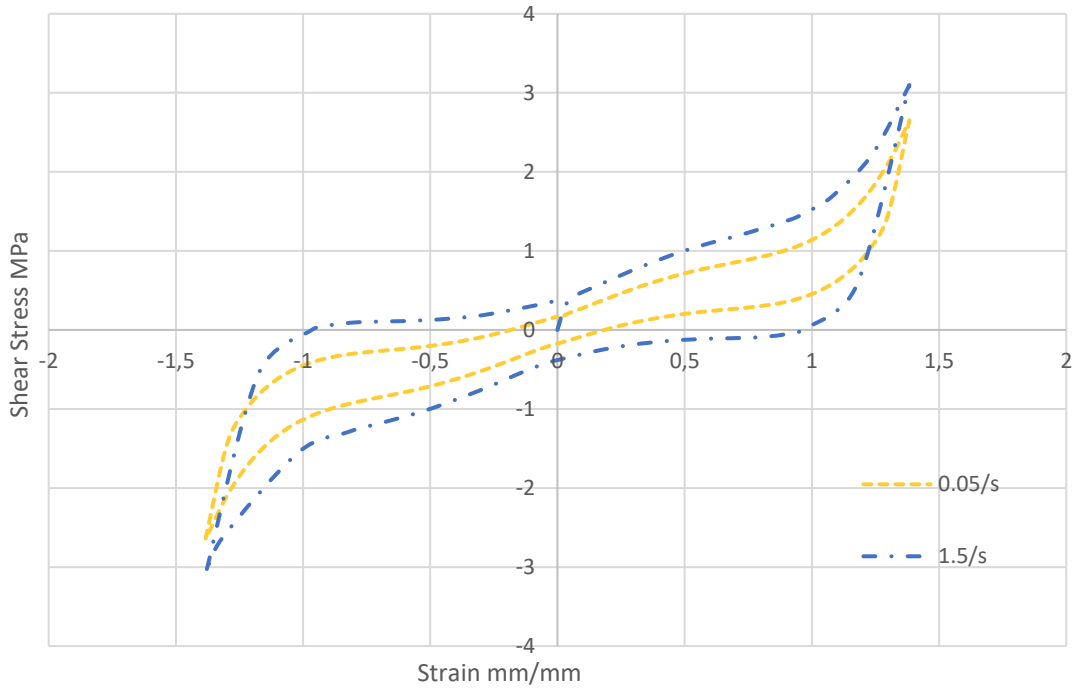

Figure 5.8. Incompressible model for different shear strain rates.

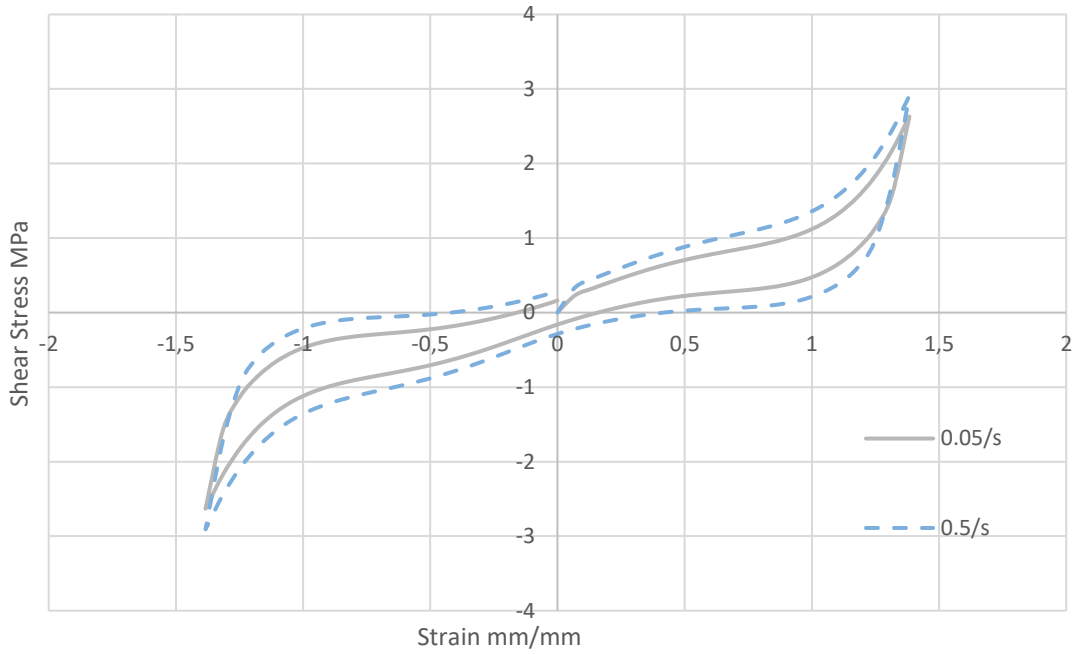

Figure 5.9. Compressibility 100 model for different shear strain rates.

5.3. Conclusions

Chapter 5 investigates behavior of full size bearing. Model result is compared with an experiment and verified for monotonic loading. Following remarks are established.

- Strain rate dependence is dominant in the rubber. Faster loading shows larger shear stiffness, dissipated energy and damping ratio compared to slower loading.
- Higher compression load results in higher damping and larger shear stiffness. This is in agreement with literature [20].
- Compressibility level of rubber affects damping ratio. Lower rubber compressibility results in higher dissipation levels.
- Analyzed bearing has shear stiffness in the range of 1.88 to 2.21. These values agree with literature which reports 1.9 to 2.94 range [9]. [7] reports range of 0.68 to 1.56 for the stiffness, lower than that predicted in this study.

- Analyzed bearing has damping ratio between 1.12 to 0.15. This is in agreement with [20] where the range is given as 0.1 to 0.28. In [2], the reported range of 0.1 to 0.14 is lower than the prediction of the model developed in this study.
- Analysis of HDRB with different shape factors showed that increasing shape factor results in higher damping and lower shear stresses.

6. CONCLUSION

In this thesis, cyclic behavior of HDR and HDRB under compression and shear are investigated through finite element analyses. Work is performed in ABAQUS software. High damping rubber is modelled to account for large strains, the rate effect and hysteresis in cyclic loading. Hyperelastic material model with hysteresis is selected over viscoelastic representation due to its computational efficiency and low number of test requirement for calibration.

For hyperelastic model Yeoh function is selected due to higher accuracy in various deformation modes. Equilibrium tests are used to calibrate Yeoh material model. To account for rate dependence, a material model accounting for rate dependence ad hysteresis is selected. Material parameters are determined from a uniaxial compression cyclic test at low strain rate.

Compression and shear response of the calibrated material model agree reasonably well with test data at various strain rates. The predicted response of HDRB for combined compression and shear loading agrees with test data up to 100% shear strain. Shear stiffness and damping ratio predictions are within the range reported in the literature.

Most of the rubber material in the industry is modelled as incompressible. If compressibility level needs to be selected, such as in using explicit solution methods, the possibility of introducing errors in the predictions should be evaluated. This study concludes that increase in compressibility reduces energy dissipation per cycle and stiffness.

Constitutive model completed in this work can further be used to determine structural responses, damping capabilities, fatigue life and possible reinforcement requirements of the isolation systems. Possible alternative designs can be further analyzed without the need of full-scale tests.

Calibration of time dependent hysteresis parameters are done by trial-error process in Chapter 3. This calibration can be further improved through optimization.

In the study, rate dependence is combined with a hyperelastic material model. Further improvement to constitutive model can be done by adding Mullin's effect. Although it is often observed that after 5 to 10 cycles, Mullin's effect perishes, contrary test results exist. Modeling of the cyclic softening in multiple cycles may be needed in such cases.

REFERENCES

1. Bhuiyan, A. R. and Y. Okui, *Earthquake Engineering*, IntechOpen, Ohio, 2012.

2. Alotaibi, E., N. Nassif, R. AlSodi, S. Ayman and I. H. Fattouh, "Assessment of Hyper-Viscoelastic Seismic Isolator Behaviour Using Finite Element" *The 4th World Congress on Civil, Structural, and Environmental Engineering Conferance*, Rome, Italy, 2019.

3. Amin, A.F.M.S., A. Lion, S. Sekita and Y. Okui, "Nonlinear Dependence of Viscosity in Modelling the Rate-Dependent Response of Natural and High Damping Rubbers in Compression and Shear: Experimental Identification and Numerical Verification", *International Journal of Plasticity,* Vol. 22, No. 9, pp. 1610-1657, 2006.

4. Amin, A.F.M.S., A. R. Bhuiyan, T. Hossain and Y. Okui, "Nonlinear Viscosity Law in Finite-Element Analysis of High Damping Rubber Bearings and Expansion Joints", *Journal of Engineering Mechanics,* Vol. 141, No. 6, pp. 1610-1657, 2015.

5. Bhuiyan, A.R., Y. Okui, H. Mitamura and T. Imai, "A Rheology Model of High Damping Rubber Bearings for Seismic Analysis", *International Journal of Solids and Structures,* Vol. 46, No. 7-8, pp. 1778-1792, 2009.

6. Konstantinos, K., M. Stergios and K. Konstantinos, "Numerical Study on the Response of Steel-Laminated Elastomeric Bearings Subjected to Variable Axial Loads and Development of Local Tensile Stresses", *Engineering Structures,* Vol. 134, pp. 346-357, 2017.

7. Murota, N., S. Suzuki, T. Mori, K. Wakishima, B. Sadan, C. Tuzun, F. Sutcu and M. Erdik, "Performance of High-Damping Rubber Bearings for Seismic Isolation of Residential Buildings in Turkey", *Soil Dynamics and Earthquake Engineering,* Vol. 143, p. 106620, 2021.

8. Saedniya, M. and S. B. Talaeitaba, “Numerical Modeling of Elastomeric Seismic Isolators for Determining Force-Displacement Curve for Cyclic Loading”, *International Journal of Advanced Structural Engineering*, Vol. 11, No. 3, pp. 361-376, 2019.

9. Nguyen, D. A., J.Dang, Y.Okui, A.F.M.S.Amin, S.Okada, T.Imai, “An Improved Rheology Model for the Description of the Rate Dependent Cyclic Behavior of High Damping Rubber Bearings”, *Soil Dynamics and Earthquake Engineering*, Vol. 77, No. 10, pp. 416-431, 2015.

10. SIMULIA Inc. ABAQUS, “Hyperelastic Behavior of Rubberlike Materials 6.14 Documentation”, http://130.149.89.49:2080/v6.10ef/books/usb/default.htmstartat=pt05ch19s05abm07.html, accessed on August 23, 2022.

11. Kelly, J. M., *Earthquake-Resistant Design with Rubber*, Springer, London, 1997.

12. Han, X. and G. P. Warn, “Mechanistic Model for Simulating Critical Behavior in Elastomeric Bearings”, *Journal of Structural Engineering*, Vol. 141, No. 5, p. 4014140, 2015.

13. Bergstrom, J. S., and M. C. Boyce, “Constitutive Modeling of the Large Strain Time-Dependent Behavior of Elastomers”, *Journal of the Mechanics and Physics of Solids*, Vol. 46, No. 5, pp. 931-954, 1998.

14. SIMULIA Inc. ABAQUS, “ABAQUS 17.8 Documentation”, https://classes.engineering.wustl.edu/2009/spring/mase5513/abaqus/docs/v6.6/books/usi/pt03ch17s08.html, accessed on September 15, 2022.

15. Amin, A. F. M. S., S. I. Wiraguna, A. R. Bhuiyan, and Y. Okui, “Hyperelasticity Model for Finite Element Analysis of Natural and High Damping Rubbers in Compression and Shear”, *Journal of Engineering Mechanics*, Vol. 132, No. 1, pp. 55-64, 2006.

16. Hamzeh, O. N., J. L. Tassoulas, and E. B. Becker, “Behavior of Elastomeric Bridge Bearings: Computational Results”, *Journal of Bridge Engineering*, Vol. 3, No. 3, p. 140–146, 1998.

17. Quaglini, V., Dubini P. and Vazzana G., “Experimental Assessment of High Damping Rubber Under Combined Compression and Shear”, *Journal of Engineering Materials and Technology*, Vol. 138, p. 011002, 2016.

18. Nguyen, H. H., and J. L. Tassoulas, “Directional Effects of Shear Combined with Compression on Bridge Elastomeric Bearings”, *Journal of Bridge Engineering*, Vol. 15, No. 1, pp. 73-80, 2010.

19. International Organization for Standardization (ISO), *Elastomeric Seismic-Protection Isolators-Part 3: Applications for Buildings*, Standard No. ISO 22762, 2018.

20. Troy, M., W. Andrew and T. Andrew, “Cyclic Behavior of High-Damping Rubber Bearings” *Fifth World Congress on Joints, Bearings and Seismic Systems for Concrete Structures*, Rome, Italy, 2001.

21. Yun, C., C. Chao, M. Qianqian, J. Huanjun and W. Zhiwei, “Study on mechanical properties of high damping viscoelastic dampers”, *Advances in Structural Engineering*, Vol. 22, No. 14, pp. 2925-2936, 2019.

APPENDIX A: MESH CONVERGENCE STUDY FOR BEARING

The mesh convergence study for the mid-sized bearing with shape factor of 12 is done for the incompressible model. For the global responses in the study, the number of elements in Figure 5.2 is doubled in the horizontal direction. The refined mesh is shown in Figure A.1.

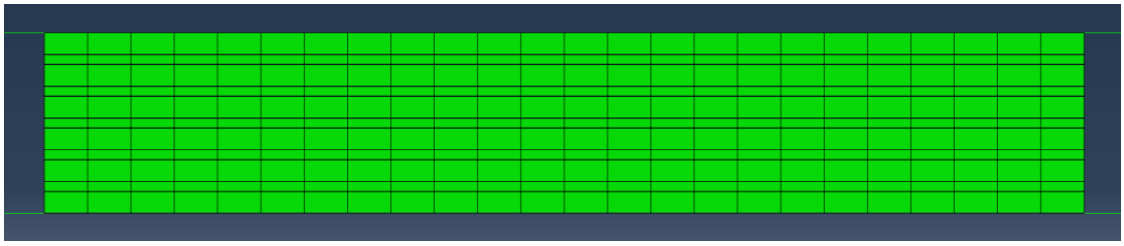

Figure 5.2. Meshed full-size bearing model.

Compression stress of 6 MPa is applied at strain rate of 0.001/s. 1.42 shear strain is applied at the rate of 0.05/s.

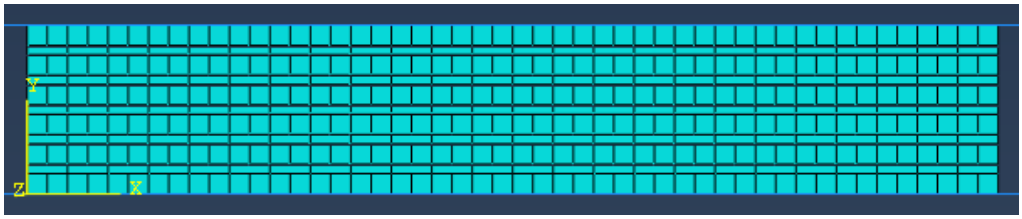

Figure A.1. Bearing model with 48 elements in horizontal direction.

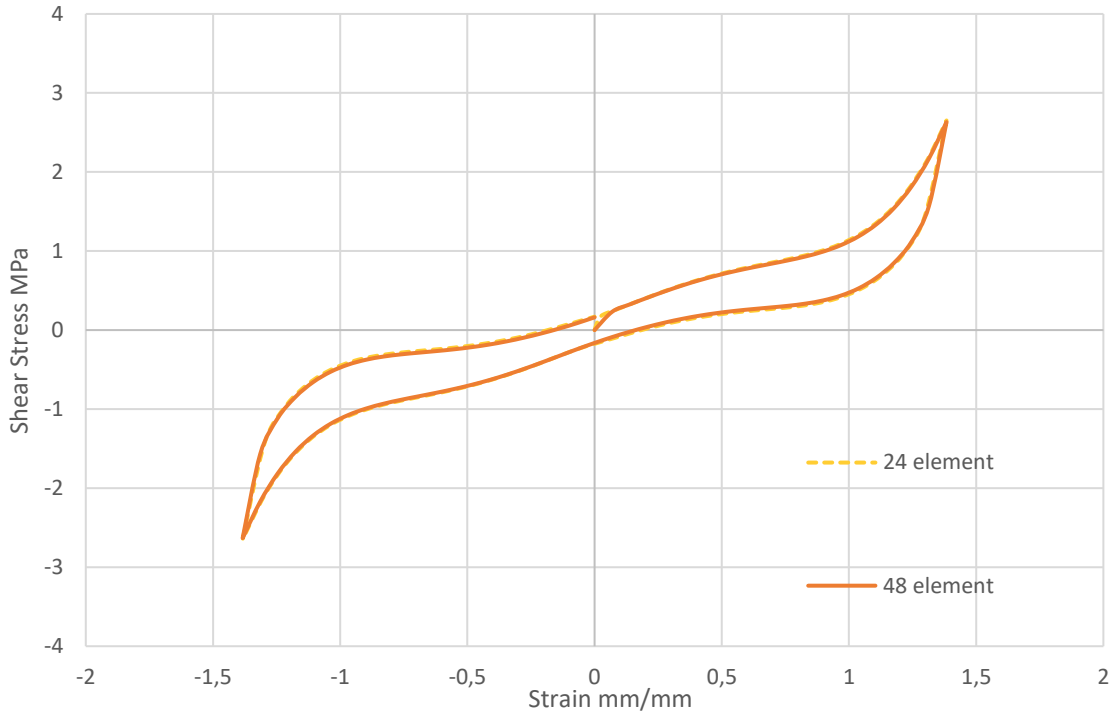

Figure A.2. Shear strain rate 0.05/s models with different element densities.

The predicted shear response shown in Figure A.2 concludes that the mesh with 24 elements is sufficient.